Algorithm Theoretical Basis Document for GOME Total Column Densities of Ozone and Nitrogen Dioxide

UPAS/GDOAS: GDP 4.0

Doc.No.: ERSE-DTEX-EOPG-TN-04-0007
Iss./Rev.: 1/A
Date: 15 December 2004

Deutsches Zentrum für Luft und Raumfahrt e.V. – DLR
Oberpfaffenhofen, Germany

Signatures

Action: Name	*Affiliation*	*Function*	*Date*	*Signature*
prepared by: R.J.D. Spurr M. van Roozendael D.G. Loyola R.	 SAO BIRA DLR-MF	 GDOAS Scientist GDOAS Scientist UPAS Scientist	15 December 2004	
released by: D.G. Loyola R.	 DLR-MF	 DLR Proj. Manager	15 December 2004	
authorized by: C. Zehner	ESA-ESRIN	ESA Proj. Manager	15 December 2004	

Distribution List

Function	*Organization*
UPAS Team	DLR-MF, DLR-DFD
GOME Team	ESA, BIRA, SAO, AUTH, various
O3M-SAF Team	EUMETSAT, FMI, various

Document Change Log

Issue	*Rev.*	*Date*	*Section*	*Description of Change*
1	A	15 December 2004	All	Completely new

TABLE OF CONTENTS

1. INTRODUCTION

1.1 Purpose and Scope

This document describes the GOME Data Processor Version 4.0 (GDP 4.0), a new operational algorithm for the retrieval of total columns of trace gases (O_3 and NO_2) from the GOME instrument. GDP 4.0 is based on the GDOAS algorithm. GDOAS is a DOAS-style algorithm developed in 2003 for the ERS ITT AO/1-4235/02/I-LG, as part of the GODFIT project (GOME DIrect Fitting) carried out by the successful BIRA/SAO consortium. Following the ITT Final Review in January 2004, GDOAS was selected for fast installation and implementation in the UPAS processing system at DLR, and subsequent deployment in the reprocessing of the entire 9-year GOME total ozone record in the second half of 2004. The operational UPAS/GDOAS algorithm has now become Version 4.0 of the GOME Data Processor (GDP); it supersedes the latest official release (GDP 3.0) at DLR.

The determination of slant column ozone is performed with a classical least-square fit based on the Beer-Lambert law; this part of GDP 4.0 is little changed from previous versions. In GDP 4.0, ozone AMF computations and the corresponding conversions to vertical column densities (VCD) are performed iteratively based on column-classified ozone profile climatology. By contrast with GDP 3.0, which used fast look-ups based on neural-network ensembles, all AMFs in Version 4.0 are calculated "on-the-fly" with calls in real time to the LIDORT radiative transfer model. For ozone, GDP 4.0 also incorporates a new molecular Ring effect correction developed at BIRA; this correction (which depends on the AMF) is applied repeatedly to the fitted effective slant column as it appears in the AMF/VCD iteration. In contrast with earlier GDP versions using ICFA data, GDP 4.0 delivers on-line cloud information (cloud-top height and albedo, fractional cover) in a pre-processing step by calling the OCRA/ROCINN cloud property algorithms.

In addition to the main technical description, this document contains sections on operational installation, dealing in particular with verification and performance issues, and error and sensitivity testing. Details of the validation of the algorithm (against ground-based and other sources) are described in a separate Validation Report [R12], but a digest of validation methods along with earlier GDOAS validation results are included in the ATBD for completeness.

1.2 Background

1.2.1 Heritage for the GDOAS algorithm

Accurate global ozone records from passive remote sensing observations play a vital role in ozone trend analysis and climate change studies. Long-term global monitoring of total ozone from satellite-borne UV spectrometers is currently in a transitional phase. The GOME (Global Ozone Monitoring Experiment) was launched on board the ERS-2 satellite in April 1995 and it is still operational. GOME-2 is scheduled for launch in early 2006 on board the first METOP satellite. The TOMS total ozone record dates back to 1978, but has become irregular from the late 1990s onwards; the next related project with NASA is the Ozone Monitoring Instrument (OMI), launched on the EOS-AURA platform in mid-July 2004.

GOME has been producing global distributions of total ozone for nine years (from July 1995), but data has been sporadic since July 2003 due to problems with tape storage on ERS-2. Also, GOME Level 1 data quality has deteriorated considerably in the last two years, mainly due to instrument degradation. The length of GOME total ozone data record makes it desirable for use in long-term ozone trend monitoring. This kind of analysis requires an accurate data record (ability to measure 1% change in total ozone concentrations globally over a period of 10 years). The intention is to include a climate data record of GOME total ozone in the next WMO ozone assessment report (2006). To this end, ESA-ESRIN issued an Invitation to Tender (ITT) in June 2002 to develop improved GOME total ozone column retrieval algorithms capable of producing trend-quality data. Three institutes were awarded contracts to perform this work in competition. The Final Review Board met in December 2003, and a further delta validation was finished in January 2004.

All three consortia studies resulted in qualitatively equivalent data products for ozone. The GDOAS algorithm (developed by the BIRA-IASB/SAO consortium) is the one most readily adaptable to operational needs, and the Review Board recommended GDOAS for implementation in the D-PAF at DLR as part of a major operational upgrade of the GOME Data Processor for improved total ozone columns. This new UPAS/GDOAS: GDP 4.0 processor system has become part of the ESA ERS Ground Segment in 2004. Although the main emphasis is on the total ozone product, the reprocessing in 2004 has also been performed on the GOME total NO_2 data record.

A joint proposal for the implementation and validation of this system and for the subsequent complete reprocessing of the entire GOME total ozone record was made in March 2004 to ESA. The proposal covered the 8-month period from April to December 2004, with Phase I (4 months) for implementation and testing, Phase II (2 months) for algorithm validation, and Phase III (2 months) for the reprocessing itself. The present document is the final version of the GDP 4.0 Algorithm Theoretical Basis Document (ATBD) and is a deliverable for Phase III of the project.

1.2.2 GOME instrument overview

The Global Ozone Monitoring Experiment (GOME) is an across-track nadir-viewing spectrometer on board the Second European Remote Sensing Satellite (ERS-2) platform launched in April 1995. It has been operating successfully for 9 years. The satellite is sun-synchronous and polar orbiting, with a period of about 100 minutes and a local equator crossing time of 10.30h, a semi-major axis of 7150 km, and a repeat cycle of 35 days. In normal viewing mode, there are three forward scans followed by a back scan, with forward scan footprint size of 320x40 km for a 1.5-second detector readout integration time; the maximum swath is 960 km, with nominal scan angle ±31° at the spacecraft. With this read-out strategy, global coverage is achieved at the equator within three days. There is also a polar viewing mode for improved sounding of polar latitudes during springtime. A comprehensive description of the GOME instrument can be found in the GOME Users Manual [R6].

GOME has 3584 spectral channels distributed over four serial-readout detectors; the wavelength range is 240 to 793 nm, with a moderate spectral resolution of 0.2 to 0.4 nm. In addition to the regular measurements of backscattered light from the Earth-atmosphere system, GOME has a Pt-Ne-Cr lamp for on-board wavelength calibration, and also a diffuser plate for the determination of solar irradiance from space (this is done on a daily basis). GOME has also three broadband (> 100 nm) Polarization Measurement Devices (PMDs) measuring light in a direction parallel to the slit. The PMDs' main purpose is to generate a polarization correction for the level 1 spectra (calibrated and geolocated radiances).

The spectral resolution of GOME is fine enough to resolve the trace gas absorption signatures of chemically important atmospheric trace species. Ozone column and profile distributions are the main mission targets, but the instrument also retrieves total columns of a number of minor trace species (NO_2, HCHO, BrO, SO_2 and OClO), total water vapor content, and some ancillary information on clouds and aerosols. The main operational Level 2 products are the global distributions of total vertical column amounts of ozone and nitrogen dioxide. For an overview of mission targets, see [Burrows et al., 1999b].

The GOME Data Processor (GDP) at the ESA Processing and Archiving Center at DLR [Loyola et al., 1997] has been operational since August 1996 following the GOME commissioning phase, and the entire data record since July 1995 has now been re-processed following upgrades (GDP Level 1-to-2 Versions 2.4 and 2.7 and 3.0) to the original retrieval algorithm.

1.3 Overview of GDP total column algorithms

1.3.1 GDP versions up to 4.0

There are four GDP versions including the present one (see Table 1).

Table 1. GDP versions, release date and product revision.

GDP Version	Release Date	Product Revision
GDP 2.0	August 1996	01
GDP 2.7	December 2000	02
GDP 3.0	July 2002	03
GDP 4.0	December 2004	04

All GDP versions up to the present have used a single contiguous fitting window from 325 nm to 335 nm covering part of the O_3 Huggins bands absorption features. The initial GDP total ozone algorithms used O_3 cross-sections from literature [Bass and Paur, 1984], but in version 3.0, the GOME-measured flight model cross-sections [Burrows et al., 1999a] were used. Versions 2.7 and earlier also assumed a single effective temperature input to be used for the temperature dependency of the O_3 cross-sections. A more recent approach [Richter and Burrows, 2002] uses two O_3 reference cross-sections to retrieve an effective temperature in addition to the slant column, and this technique was incorporated in version 3.0. NO_2 DOAS fitting in all versions has used a fitting window in the visible from 425 nm to 450 nm. As with O_3, literature cross sections used in versions 2.0 and 2.7 were replaced in version 3.0 by GOME flight model NO_2 cross-sections [Burrows et al., 1998].

In GDP 3.0, the use of pre-shifted O_3 and NO_2 cross-sections was implemented, with an explicit shift fitting only for the orbital solar spectrum re-sampled to the earthshine spectra observational wavelength grids. In the UV, GOME samples slightly below the Nyquist criterion, and an undersampling correction reference spectrum was introduced in Version 3.0 to compensate for this effect [Slijkhuis et al., 1999; Chance, 1998]. Up to version 2.7, Ring effect interference was treated using a single Ring reference spectrum derived from pre-launch GOME zenith sky measurements. Versions 3.0 and later used a theoretical Ring Fraunhofer spectrum derived from a folding of Raman cross-sections with a high-resolution solar spectrum [Chance and Spurr, 1997]. A correction for molecular Ring interference effects has now been introduced for GDP 4.0 total ozone (see section 2.4).

For O_3 in GDP 2.0 and 2.7 and for NO_2 in GDP 2.0, 2.7 and 3.0, *single-scatter* AMFs were computed from scratch, with multiple scatter corrections interpolated from large look-up tables (LUTs) classified according to scenario geometry and various atmospheric parameters. These look-up tables were calculated using the GOMETRAN radiative transfer model [Rozanov et al., 1997].

A new O_3 AMF implementation was written for GDP 3.0, based on an iterative adjustment to AMF and Vertical Column Density (VCD) to reflect the actual ozone content as expressed through the fitted slant column [Spurr, 1999]. O_3 AMFs were prepared beforehand using the

LIDORT radiative transfer (RT) model [Spurr, 2002], with resulting LUTs then used to train neural network ensembles for fast computation of AMF values [Loyola, 1999]. By contrast, GDP 4.0 uses "on-the-fly" LIDORT radiative transfer AMF computations – modern computing power is now sufficient to achieve data turnover in real time.

In addition to the basic Level 1 input of calibrated geolocated earthshine measurements (radiances) and solar irradiance, GDP requires inputs from a pre-processing cloud property algorithm in order to deal with partially cloudy scenes in the independent pixel approximation (IPA). All versions to date have taken fractional cover retrieved by the Initial Cloud Fitting Algorithm (ICFA) [Kuze and Chance, 1994] based on fitting of reflectance measurements in and around the O_2 *A* band, and cloud-top pressure supplied from the international satellite cloud climatology project (ISCCP) data base [Schiffer and Rossow, 1983]. GDP 4.0 uses the OCRA/ROCINN cloud algorithm for providing this ancillary information.

The first major GDP total ozone validation was done in 1998 using ground-based (NDSC and SAOZ networks) data and results from the Total Ozone Mapping Spectrometer (TOMS) [Lambert et al., 1999; Lambert et al., 2000]. Validation results revealed some biases and regional discrepancies, in particular at high latitudes and high solar zenith angles, and for situations with high or low ozone content. A further "delta" validation (ground-based only) was performed in 1999 on Version 2.7 to check NO_2 algorithm improvements.

A second major validation was performed in 2002 on GDP 3.0 with significant improvements across the board [Lambert et al., 2002]. A set of some two thousand previously validated orbits was used (sampled over a 4-year time period). Validation tools and ground-based data already set up for previous delta validations were used again. The complete GOME total O_3 and NO_2 data records from July 1995 as reprocessed with GDP 3.0 are publicly available.

1.3.2 GDOAS: relation to GDP 3.0

An ESA-sponsored sensitivity study and validation [R7] of the GDP 3.0 algorithm was carried out in 2002 and several improvements were suggested therein [van Roozendael et al., 2002]. This exercise led in turn to the ESA ITT study for improved GOME total ozone algorithms, and the subsequent selection of the GDOAS algorithm for major reprocessing of the GOME record. GDOAS has now been implemented operationally into the UPAS system, and the result is the GDP 4.0 software system.

In order to provide some context, we outline here the main differences between GDP 4.0 and GDP 3.0. Of relevance here is the interim software requirements document [R4] prepared in March 2004, and intended as a bridge between the GODFIT/GDOAS project work in 2003 and the UPAS/GDOAS enterprise in 2004. Both versions use the standard window 325-335 nm for the DOAS fitting; also both versions use the iterative technique for AMF/VCD computation (based on the use of column-classified ozone profile climatology).

Slant column fitting. There have been some small but important changes between versions 3.0 and 4.0. The wavelength calibration has been improved, and a different shift/squeeze scheme adapted for wavelength registration of level 1 data (solar spectrum is now the reference). All fitting includes amplitudes for Fraunhofer Ring effect and undersampling.

Molecular Ring effect. This correction is the most important new consideration coming from the Version 3.0 sensitivity study. A new correction has been implemented in GDP 4.0 and is given a detailed description in the present document.

Air Mass Factors. In GDP 3.0, LIDORT simulations and parameterized look-up tables based on neural network ensembles were used for AMF generation, and O_3 AMFs were pre-calculated at 325.0 nm. By contrast in GDP 4.0, all ozone AMFs in GDOAS are computed from on-the-fly simulations with LIDORT; there are no look-up tables. Also, the wavelength 325.5 nm is now used following a recommendation in the 2002 ESA study [R7]. GDP 3.0 used the TOMS V7 O_3 profile set, while GDP 4.0 uses the recently released TOMS V8 climatology.

Cloud data. GDP 3.0 uses ICFA results for effective cloud fraction, and ISCCP data for cloud-top pressures. The GDOAS prototype was developed to ingest off-line FRESCO results for effective fraction and cloud-top pressure. The GDP 4.0 implementation now generates cloud information (cloud-top height and albedo, effective cloud fraction) from the OCRA/ROCINN algorithms developed in-house at DLR.

1.4 Reference Documentation

The following documents are applicable to the present ATBD:

[A1] Upgrade of the GOME Data Processor for Improved Total Ozone Columns, ERSE-ESPR-EOPS-SW-04-0001, C. Zehner, February 2004.

[A2] Space Engineering Software ECSS-E-40B, 2003.

The following documents are for reference:

[R1] GOME Direct Fitting (GODFIT) ATBD, ESA contract AO/1-4235/02/I-LG, R.J.D. Spurr and M. van Roozendael, 14 November 2003.

[R2] GOME Direct Fitting (GODFIT) Validation Report, ESA contract AO/1-4235/02/I-LG, M. van Roozendael et al., 14 November 2003.

[R3] GDOAS Delta validation report, ESA contract AO/1-4235/02/I-LG, 28 January 2004.

[R4] Interim SRD/SUM for GDOAS Implementation at DLR, ESA contract AO/1-4235/02/I-LG, Robert Spurr and Michel van Roozendael, March 2004.

[R5] Technical Description GOME Level 1b to 2 algorithm, Iss./Rev. 3/A, July 2002.

[R6] GOME Global Ozone Monitoring Experiment Users Manual, ed. F. Bednarz, ESA SP-1182, 1995.

[R7] ERS-2 GOME GDP 3.0 Implementation and Delta Validation Report, ERSE-DTEX-EOAD-TN-02-0006, Issue 1.0, November 2002.

[R8] Technical Description GOME Level 0 to 1b algorithm, Iss./Rev. 5/A, December 2000.

[R9] Ozone SAF: Design Document for the GOME-2 Universal Processor for Atmospheric Spectrometers, SAF/O3M/DLR/DD/001, October 2003.

[R10] Output Product Format Document for GOME Total Column Densities of Ozone and Minor Trace Gases, DLR/UPAS/GOME/OPF/01, Iss./Rev. 1/A, November 2004.

[R11] Product Specification Document of the GOME Data Processor, ER–PS–DLR–GO–0016, Iss./Rev. 4/B, December 2004.

[R12] Delta Validation Report for ERS-2 GOME Data Processor Upgrade to Version 4.0, ERSE-CLVL-EOPG-TN-04-0001, Issue 1.0, December 2004.

1.5 Abbreviations and Acronyms

AAIA	Absorbing Aerosol Indicator Algorithm
AMF	Air Mass Factor
BIRA-IASB	Belgian Institute for Space Aeronomy
BRDF	Bi-directional Reflectance Distribution Function
DLR	German Aerospace Center
DOAS	Differential Optical Absorption Spectroscopy
DU	Dobson Unit
ECMWF	European Center for Medium-range Weather Forecasting
ENVISAT	Environmental Satellite
EOS-AURA	(NASA's) Earth Observing System Aura
EPS	EUMETSAT Polar System
ERS-2	European Remote Sensing Satellite-2
ESA	European Space Agency
ESC	Effective Slant Column
EUMETSAT	European Organization for the Exploitation of Meteorological Satellites
FOV	Field of View
FRESCO	Fast REtrieval Scheme for Clouds from the Oxygen *A*-band
GAW	Global Atmospheric Watch
GDOAS	GODFIT-DOAS
GDP	GOME Data Processor
GOME	Global Ozone Monitoring Experiment
ICFA	Initial Cloud Fitting Algorithm
IMF	Remote Sensing Technology Institute
IPA	Independent Pixel Approximation
LIDORT	Linearized Discrete Ordinate Radiative Transfer
LOS	Line-of-Sight
METOP	Meteorological Operational
NDSC	Network for the Detection of Stratospheric Change
NN	Neural Network
OCRA	Optical Cloud Recognition Algorithm

OMI	Ozone Monitoring Instrument
PMD	Polarization Measurement Device
RMS	Root Mean Square
ROCINN	Retrieval of Cloud Information using Neural Networks
RRS	Rotational Raman Scattering
RTM	Radiative Transfer Model
SAO	Smithsonian Astrophysical Observatory
SCIAMACHY	SCanning Imaging Absorption spectroMeter for Atmospheric CartograpHY
SZA	Solar Zenith Angle
TOA	Top of Atmosphere
TOMS	Total Ozone Mapping Spectrometer
UV	Ultra Violet
UKMO	United Kingdom Meteorological Office
UPAS	Universal Processor for UV/VIS Atmospheric Spectrometers
VCD	Vertical Column Density
VIS	Visible
WMO	World Meteorological Office
WOUDC	World Ozone and Ultraviolet Data Center

1.6 Document Overview

Section 2 contains the main ATBD description. In section 2.1, we give an overview of the GDOAS algorithm and outline the major algorithm components. The main focus is on the total ozone algorithm (sections 2.2 – 2.4).

The DOAS algorithm (section 2.2) is based on earlier technical algorithm descriptions issued for GDP [R5], major updates for version 3.0 are noted here along with more recent changes. Section 2.3 concerns determination of Air Mass Factors (AMFs) and Vertical Column Densities (VCDs) of total column. This section discusses the necessary radiative transfer computations, and gives a summary description of the LIDORT scattering code. Some descriptions in this section have been adapted from text used in the GODFIT ATBD [R1]; see also [Spurr et al., 2004]. The molecular Ring correction for O_3 is one of the key improvements from GDP 3.0, and this is discussed in detail in section 2.4. This section also summarizes the use of off-line RT models with an inelastic rotational Raman scattering (RRS) capability used in closed-loop testing of the new Ring effect parameterization. Section 2.5 summarizes the GDOAS algorithm for NO_2 columns, while section 2.6 contains some notes on the cloud pre-processing algorithms. Section 2.7 summarizes the error computation for total ozone.

Section 3 concerns operational implementation of GDOAS in the UPAS system. We first give a brief overview of the UPAS system and its capability (section 3.1). In section 3.2, we discuss GDOAS implementation issues, including pre-processing steps (wavelength registration, cloud ingestion or pre-processing, etc.), and the handling of input and output. Section 3.2 is also devoted to verification of the GDOAS/UPAS implementation, and includes a number of issues on comparison of in-house code with external GDOAS code from 2003.

Section 4 introduces the GDP 4.0 validation and deals with some sensitivity issues. Section 4.1 discusses some sensitivity tests for GDP 4.0, as carried out on the GDOAS algorithm in preparation for the Final Review Board assessment in January 2004. In section 4.2 we note briefly the validation tools and methodology, and we give a digest of the main findings of the GDP 4.0 validation campaign. The detailed Validation Report for GDP 4.0 [R12] will be presented separately as an accompanying document to the present ATBD.

2. ALGORITHM DESCRIPTION

2.1 GDOAS overview

The flowchart in Figure 1 gives an overview of the GDOAS algorithm for total ozone retrieval. The granularity is assumed to be one orbit. In other words, a whole orbit of level 1 data is ingested before any processing takes place, and an orbit's worth of Level 2 data is written to file after the granule has been processed.

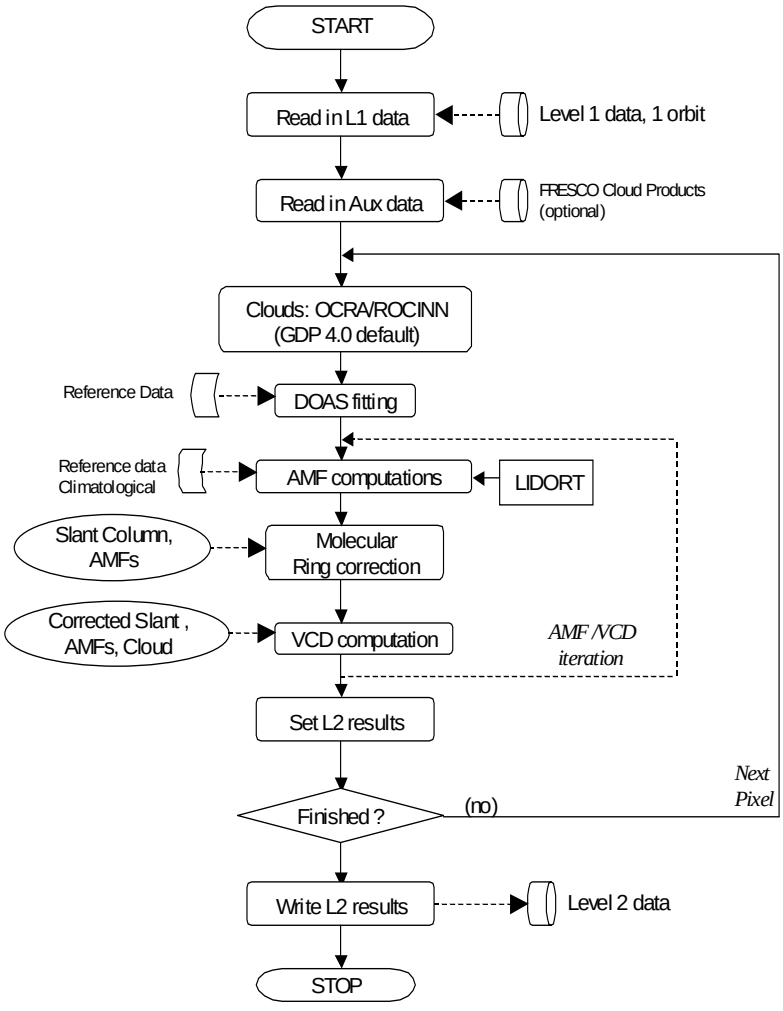

Figure 1. Logical structure of the GDOAS algorithm; granularity 1 orbit.

The first algorithm component is the DOAS Fitting; this delivers the effective slant column of total ozone, plus a number of auxiliary fitted parameters and error diagnostics. The second component is the iterative AMF/VCD computation to generate the final vertical column of total ozone. At each step, AMFs are first computed for the current guess of the vertical

column; the slant column is then corrected using the Molecular Ring correction, and used (together with cloud information and AMF results) to update the VCD guess.

For NO_2, the GDOAS process is simpler; there is no AMF/VCD iteration, and no molecular Ring correction. The DOAS slant column fitting result is used immediately in a single AMF conversion to the vertical column. For details, see Section 2.5.

The pixel processing is completed with an assignation of the L2 output (total column, errors and diagnostics, auxiliary output). Note the two options for ancillary cloud information: (a) cloud algorithm products derived from internal calls to the OCRA/ROCINN algorithms (the operational baseline); and (b) auxiliary data created offline using the FRESCO algorithm and ingested in granular units.

2.2 The DOAS algorithm in GDP 4.0

2.2.1 DOAS fitting method

The DOAS (Differential Optical Absorption Spectroscopy) fitting method was first used over 20 years ago for the determination of slant column amounts from sky measurements taken by UV and visible ground-based spectrometers. Following extensive ground-based applications, DOAS was selected for GOME total ozone retrieval in August 1992 and implemented operationally in 1995. DOAS uses least-squares minimization for the fitting of atmospheric and related parameters.

In DOAS, the atmospheric model is based on the Beer-Lambert extinction law for trace gas absorbers. This is a reasonable model to use for optically thin trace gas absorption in the atmosphere, where the cross-sections are weakly dependent on pressure, and may possess a strong linear dependence on temperature. In DOAS, it is standard practice to use logarithms of intensities (optical densities), and then add an external closure term in the form of a low-order polynomial (typically of degree 2) to account for broadband molecular and aerosol scattering and also for reflection from the Earth's surface. The fitting model is then:

$$Y(\lambda) \equiv \ln\left[\frac{I_\lambda(\Theta)}{I_\lambda^0(\Theta)}\right] = -\sum_g E_g(\Theta)\sigma_g(\lambda) - \sum_{j=0}^{3} \alpha_j \left(\lambda - \lambda^*\right)^j . \qquad (1)$$

Here, I_λ is the earthshine spectrum at wavelength λ, and for GOME, I_λ^0 is usually taken to be the extraterrestrial solar spectrum. This model applies to trace gas absorption through the whole atmosphere, where $E_g(\Theta)$ is the *effective* slant column density of gas *g* appropriate to an atmospheric path characterized by geometrical path Θ, and $\sigma_g(\lambda)$ is the associated trace gas absorption cross section. α_0, α_1, α_2 and α_3 are coefficients for the low-order polynomial filter (a cubic has been assumed), with λ^* a reference wavelength for this polynomial.

The chi-square merit function in the fitting is a weighted least squares difference between measured and simulated optical densities $Y_{meas}(\lambda)$ and $Y_{sim}(\lambda)$ respectively. The weighting in this function is the inverse of the square of the relative optical density measurement error; the latter quantity may be expressed easily in terms of absolute errors on the solar and earthshine

measurements. For a review of the DOAS method and some of its applications, see [Platt, 1994].

Leaving aside issues of wavelength registration, Eq. (1) is linear in the fitting variables $E_g(\Omega)$ and $\{\alpha_k\}$, and the minimization is then multi-linear regression. Additional reference spectra may be considered in the fitting, to compensate for instrumental effects such as undersampling, and atmospheric effects due to inelastic rotational Raman scattering (the Ring effect); these terms are additive (thus maintaining the linearity). Wavelength mismatching is often dealt with by applying shift and squeeze parameters to the wavelength grids of the reference spectra, and also to the measurement (solar and earthshine) spectra. Shift and squeeze parameters may be fitted, in which case the fitting is then iteratively non-linear in these parameters. The embedded DOAS multi-linear regression is then repeated for all iterations, until convergence is reached for the re-sampling parameters. More details may be found in [R5]. Experience with the GOME DOAS fitting has shown that it is desirable wherever possible to use pre-established shifts and squeezes to speed up the performance, and reduce the possibility of numerical instability. We return to these issues below.

Over the lifetime of GOME, a number of improvements have been made to the original DOAS algorithm, following essential research by a number of groups associated with the instrument. Improvements for the total ozone algorithm are discussed in the following two subsections dealing with DOAS implementation; baseline UPAS/GDOAS values are mentioned in the text. DOAS issues for the NO_2 algorithm are discussed separately in Section 2.5.

2.2.2 Effective temperature fitting

Ozone cross sections in the Huggins bands are strongly temperature dependent [Paur and Bass, 1984], and this must be treated in the fitting. Before GDP 3.0, a single ozone cross-section was used as the trace gas reference spectrum, and temperature dependence was dealt with by assuming a single effective temperature T_{eff}. This number was selected from climatology, as being the temperature at that pressure level which corresponds to the maximum number density in the appropriate climatological ozone profile.

However, a significant improvement in the DOAS fit was found with the use of two ozone cross-sections at different temperatures [Richter and Burrows, 2002]. This procedure, which was first suggested by A. Richter (Uni. Bremen), allows for linear adjustment of the slant column retrieval to the actual O_3 profile weighted-mean atmospheric temperature [van Roozendael et al., 2002]. We retrieve T_{eff} in addition to the effective slant column, thus avoiding the potentially large source of uncertainty associated with an externally imposed choice of effective temperature. Specifically, we use the ozone cross-section at temperature T_1, plus an ozone *difference* cross-section (between temperatures T_1 and T_2), and the temperature dependence of the complete cross-section is assumed to be:

$$\sigma(T) = \sigma(T_1) + (T - T_1)\frac{\partial \sigma}{\partial T} \approx \sigma(T_1) + (T - T_1)\frac{\sigma(T_1) - \sigma(T_2)}{(T_1 - T_2)}. \qquad (2)$$

The dependence is linear if we assume the temperature derivative is constant. This assumption is largely valid over the limited range of stratospheric temperatures. Taking T_1 =

221 K and T_2 = 241 K, so that $\Delta T = T_1 - T_2 = 20$ K, we use $\sigma(T_1)$ and $\Delta\sigma_{12} = \sigma(T_1) - \sigma(T_2)$ as the reference spectra in the fitting. The total slant column optical depth is $E.\sigma(T)$, for effective slant column density E, which is then the fitting parameter corresponding to $\sigma(T_1)$. The other fitting parameter D corresponds to the difference cross sections $\Delta\sigma_{12}$, and from knowledge of the two parameters D and E, we can define a retrieved effective temperature through the relation:

$$T_{eff} = T_1 + (T_1 - T_2)\frac{D}{E} \quad . \tag{3}$$

Effective slant columns are now independent of any assumed temperature climatology. The retrieved temperature varies with latitude and season, and for diagnostic purposes, values can be compared not only with climatological data but also with analysis fields from forecast models.

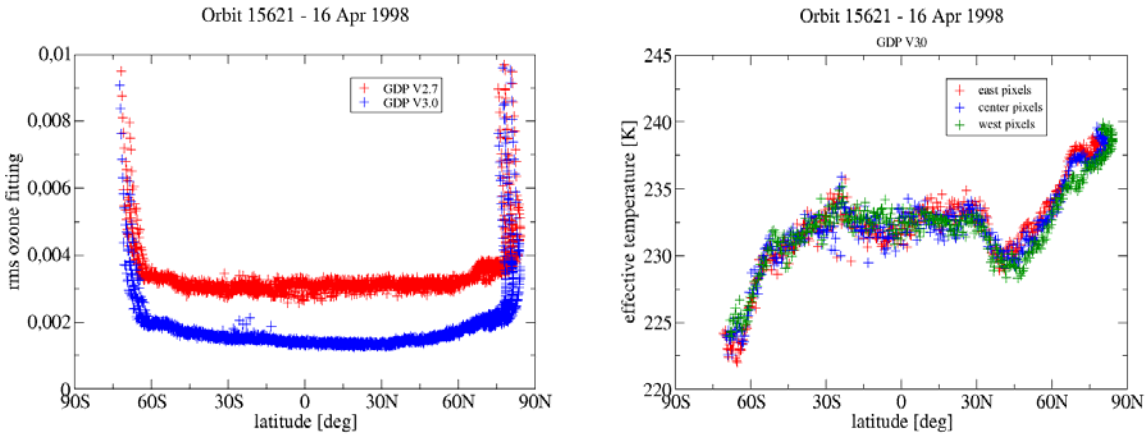

Figure 2. (Left) Improvement from version GDP 2.7 to GDP 3.0 in the fitting RMS for a single orbit of GOME data. (Right) Fitted effective temperatures for the same orbit. Taken from [R7].

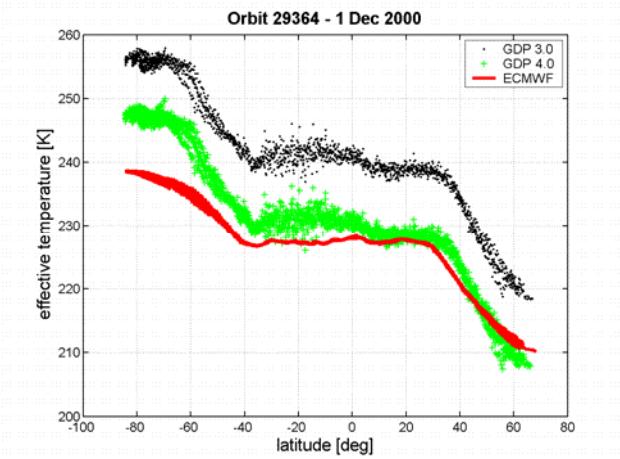

Figure 3: Retrieved effective temperature for O_3 cross-sections derived from GDP V3.0 (dots) and GDP V4.0 (green), and compared with ECMWF analysis data (solid red lines) for one GOME orbit from 1st December 2000.

In Figure 2, we illustrate these changes for a springtime orbit of GOME data. The root mean square (RMS) has improved by a factor of two almost everywhere. In the right-hand panel, fitted effective temperatures vary from 222 K to 240 K in the Northern high latitudes. These values are generally lower than ozone-maximum temperatures selected from climatology. Validation has proved consistently that the use of this fitted-temperature DOAS formalism gives better total ozone column results [Lambert et al., 2002].

In Figure 3, we compare effective ozone temperatures derived from GDP 3.0 and 4.0 with analysis data from ECMWF (ECMWF temperature fields were averaged over atmospheric height using climatology ozone profiles as weighting factors). GDP 4.0 results are much closer to the ECMWF data thus largely reducing the bias in effective temperatures.

Total column NO_2 is fitted as an auxiliary parameter in the 325-335 nm window for total ozone; a single temperature is assumed (this is 241 K, see below, and also section 2.5).

2.2.3 Reference spectra and re-sampling issues

GDP 3.0 and 4.0 use the latest released version of the GOME Flight Model cross-sections (O_3 and NO_2), the so-called GOME FM98 data [Burrows et al., 1998; Burrows et al., 1999a]. These cross-sections were derived from gas-cell calibration experiments with the GOME instrument prior to the April 1995 launch; for ozone, measurements were performed at five temperatures (202 K, 221 K, 241 K, 273 K and 293 K).

In GDP 3.0, trace gas cross-sections were subjected to a pre-shift re-sampling (the shift was 0.012 nm towards longer wavelengths for O_3 and NO_2 cross sections in the customary 325-335 nm GOME DOAS window). Although shift and squeeze fitting for these reference spectra has always been possible in GDP, this choice has been disabled in Version 3.0 in order to avoid occasional numerical instabilities found in the earlier GDP versions. This is also a strong performance consideration, since the DOAS fitting becomes multi-linear regression.

In GDP 4.0, the solar spectrum is used as the wavelength reference; for each footprint, the earthshine spectrum must be re-sampled on this reference grid by application of fitted shift and squeeze parameters. This wavelength mismatch is due mainly to the solar spectrum Doppler shift (an average shift value is 0.008 nm), and it will vary across an orbit due to changes in the instrument temperature. The shift and squeeze are the only two parameters requiring non-linear least squares fitting – at each iteration and corresponding update of this shift/squeeze combination, the DOAS multi-linear regression is performed, based on the pixel-wise division of (re-sampled) earthshine and solar spectra required for the measurement optical densities in Eq. (1). Note that this shift/squeeze scheme differs from that used in GDP 3.0 and earlier, where the solar spectrum was always re-sampled to the wavelength grid of the earthshine spectrum.

Following recommendations issued after the GOME GDP 3.0 geophysical validation campaign in 2002 [van Roozendael et al., 2002], O_3 cross-sections are now corrected for the so-called solar I_0 effect [Aliwell et al., 2002], and have been implemented with an optimized pre-shift value of +0.016 nm (instead of +0.012 nm). This applies only to the [325-335] window for total ozone. This is consistent with the wavelength calibration improvement

incorporated in UPAS/GDOAS for this window (see next paragraph). This revised pre-shift value is now the UPAS/GDOAS baseline. This change has removed a systematic positive bias of 1.5 % in GDP 3.0 total ozone, and it has also compensated a positive bias in the derived effective temperatures. In the 325-335 nm window, NO_2 cross-sections are not corrected for the solar I_0 effect, but the same optimized pre-shift value has been used.

A word is in order regarding wavelength calibration. Level 1b spectra are generated using the Level 0 to 1b extractor, which has two options for wavelength calibration: (1) application of calibration coefficients derived from in-flight line-lamp measurements, and (2) coefficients derived from cross-correlations between the GOME solar spectrum and a slit-function convolved high resolution spectrum. Details may be found in the Level 0 to 1b technical documentation [R8]. Additional improvements have been made to GOME level 1 calibrations; in particular, the GOMECAL package was prepared by KNMI for a range of GOME applications (van Geffen and van Oss, 2003).

In UPAS/GDOAS, the Level 1 product is extracted without applying the cross-correlation option of the GDP Level 0-to-1 extractor. GDP 4.0 baseline is to apply its own window-dependent pre-shifts to parts of the solar spectrum before each orbit of data is processed. These pre-shifts are established by cross-correlation with a high-resolution solar spectrum over limited wavelength ranges covering the main fitting windows (325-335 nm for O_3, 425-450 nm for NO_2 in the visible, and 758-772 nm covering the O_2 *A* band as used in the ROCINN algorithm). Figure 4 demonstrates the improved stability in O_3 fitting due to this calibration enhancement (which has been called “post Level 1 processing”).

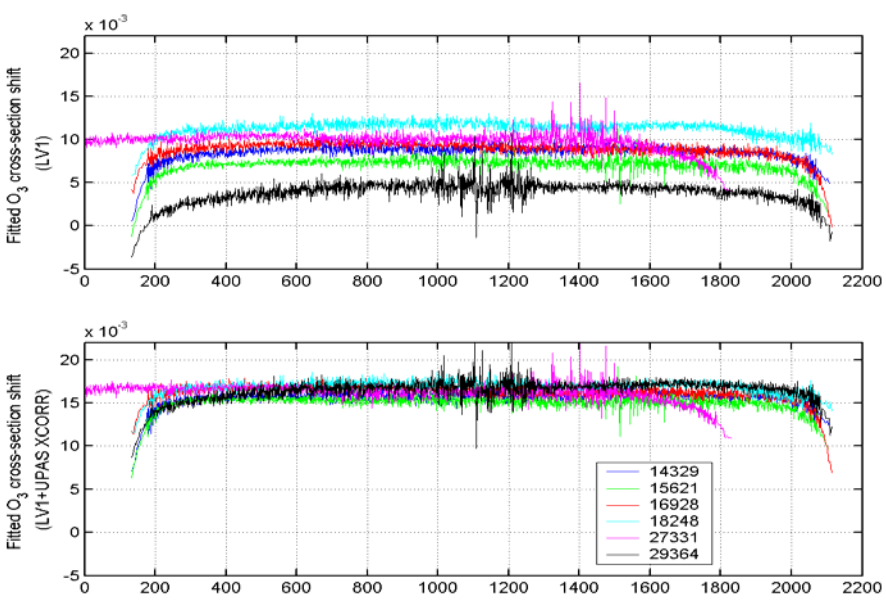

Figure 4: Improvement in fitted ozone cross-section shift resulting from additional post “Level 1” wavelength cross-correlation in UPAS.

In the UV, GOME actually samples slightly below the Nyquist criterion, and it was found that this effect could be largely compensated by the introduction of an undersampling

correction [Chance, 1998; Slijkhuis et al., 1999]. A reference spectrum was prepared to handle this effect, and is now standard from version 3.0 onwards.

2.2.4 Ring effect Fraunhofer spectrum

The Ring effect (Fraunhofer and telluric filling-in due to inelastic rotational Raman scattering) induces a small-amplitude distortion in the earthshine spectrum, first observed over 40 years ago [Grainger and Ring, 1962]. In the UV window 325-335 nm, Ring effect distortion of O_3 Huggins bands absorption features is large enough to seriously compromise total ozone fitting accuracy. In DOAS-type algorithms, Ring structures are commonly dealt with by using pre-calculated *Ring spectra*, usually defined as (logarithms) of the ratios of radiances with and without rotational Raman scattering (RRS).

Scaling parameters for additive Ring reference spectra (Fraunhofer and/or telluric effects) can be included in the DOAS fit; in this way the Ring effect is treated as "pseudo absorption". The approach adopted in GDP Version 3.0 has been to use a single theoretical Ring Fraunhofer spectrum from a folding of rotational Raman cross-sections at a fixed temperature with a high-resolution solar Fraunhofer spectrum taken from the Kitt Peak Observatory [Chance and Spurr, 1997]. This is in effect a zero-order calculation of RRS; the resulting Ring reference spectrum is often sufficient for use in DOAS fitting of (optically thin) minor trace species total columns, for which molecular filling-in can be neglected in comparison with other sources of uncertainty. The GDP 4.0 baseline in UPAS fits a single Ring scaling parameter for the additive zero-order Fraunhofer spectrum as described above.

For total ozone, attempts have been made to introduce a second Ring reference spectrum in the DOAS fitting, but this "one-size-fits-all" approach does not adequately characterize the Ring effect in a consistent manner. It has also become clear from RT modeling studies (with inelastic RRS included) that a more sophisticated approach is required.

A new molecular Ring effect correction was developed for GOME total ozone in 2002 following the GDP 3.0 study [van Roozendael, 2002]. This correction is an *ex post facto* explicit scaling of the DOAS slant column result, and it takes place after the DOAS fit, but before the AMF/VCD calculations. A full description has been given in Section 2.4 below; it is fair to say that this correction is the most important improvement from GDP 3.0, one that has finally allowed the GOME total ozone accuracy levels to approach trend analysis levels.

Note that for NO_2, we would expect a molecular Ring correction effect comparable to that for ozone, but such an error would be small in comparison with other error sources affecting the NO_2 column retrieval. This is the main reason for excluding this correction for NO_2, though implementation of the correction should be considered in the future pending appropriate investigation and verification.

2.2.5 Baseline summary for DOAS fitting (O_3, 325-335 nm)

The state vector in the DOAS *linear* regression fitting has 9 parameters:

- Effective slant column [DU] of O_3 1
- Fitting parameter for O_3 differential cross-section 1

- Effective slant column [DU] of NO_2 1
- Polynomial closure parameters 4
- Scaling factor for Fraunhofer Ring spectrum (additive) 1
- Scaling factor for undersampling spectrum (additive) 1

The state vector in the DOAS *nonlinear* least-squares iterative fitting has 2 parameters:

- Wavelength shift for re-sampling earthshine spectrum 1
- Wavelength squeeze for re-sampling earthshine spectrum 1

The pre-shifts implemented are:

- GOME FM98 O_3 cross-sections, I_0-corrected, pre-shift +0.016 nm
- GOME FM98 NO_2 cross-sections, pre-shift +0.016 nm

These 11 parameters must be fitted for each footprint. In addition, we have the "post Level 1" solar spectrum pre-shift determined at the beginning of each orbit (the value of this parameter will depend on the irradiance spectrum).

2.3 AMF and VCD determination in GDP 4.0

2.3.1 The iterative AMF/VCD method

The ozone AMF definition that has been used in all GDP Versions is the traditional one:

$$A = \frac{\log\left(I_{nog} / I_g\right)}{\tau_{vert}}. \qquad (4)$$

Two calculations of backscatter intensity are required: one (I_g) for an atmosphere including ozone as an absorber, the other (I_{nog}) for an atmosphere excluding ozone absorption; τ_{vert} is the vertical optical depth of ozone for the whole atmosphere. Other definitions have been suggested, but these have so far only been applied to GOME windows with optically thin trace gas absorbers such as HCHO and NO_2 [see for example, Palmer et al., 2001].

In GDP 3.0 and earlier versions, AMFs for total ozone column were calculated at 325 nm at the lower end of the DOAS fitting window (325-335 nm). Closed-loop tests [van Roozendael et al., 2002] have shown that with this choice of AMF wavelength, total column errors of up to 5% are possible for solar zenith angles in excess of 80°; and generally, errors at the 0.5-1% level are found for sun angles < 80°. It was recently found [van Roozendael et al., 2002] that these errors are reduced (to the 1-2% level for SZA> 80°) when 325.5 nm is used as the representative AMF wavelength. This value was adopted for the GDOAS development in 2003 as part of the GODFIT work; it is the current baseline in GDP 4.0.

For a given choice of ozone profile, we require a radiative transfer model to compute the AMF. For a clear sky scenario, the final vertical column density (VCD) is then defined as the effective slant column divided by a single AMF computed using this ozone profile.

$$V = \frac{E}{A_{clear}}, \tag{5}$$

where E is the effective slant column, and A_{clear} the clear sky AMF. For partially cloudy scenarios, AMF computations are based on the independent pixel approximation, and the conversion from slant column to VCD proceeds via the relation:

$$V = \frac{E + \Phi G A_{cloud}}{(1-\Phi)A_{clear} + \Phi A_{cloud}}, \tag{6}$$

where A_{cloud} is the AMF for the atmosphere down to the cloud-top level.

In GDP 3.0 and earlier, the factor ϕ is just the effective cloud fraction f; an alternative definition is the "intensity-weighted cloud fraction" $\Phi = fI_{cloud}/I_{total}$, where $I_{total} = (1-f)I_{clear} + fI_{cloud}$. Both definitions of Φ were implemented in GDOAS. Studies have shown that total AMFs defined with the intensity-weighted cloud fraction are more suitable for the ozone application [Martin et al., 2002];this option will be the default in the reprocessing. The "ghost column" G is the quantity of ozone below cloud-top; it must be computed from the given choice of ozone profile.

In traditional DOAS retrievals, slant column fitting and AMF calculation steps are decoupled; for a given trace species, the AMF radiative transfer computations are based on seasonally and geographically classified climatological profile inputs that may have no real connection to the true profile. This is the case with GDP versions 2.7 and earlier, where a suitable ozone profile has traditionally been interpolated (by time and latitude) from a zonal-mean monthly climatology of profiles.

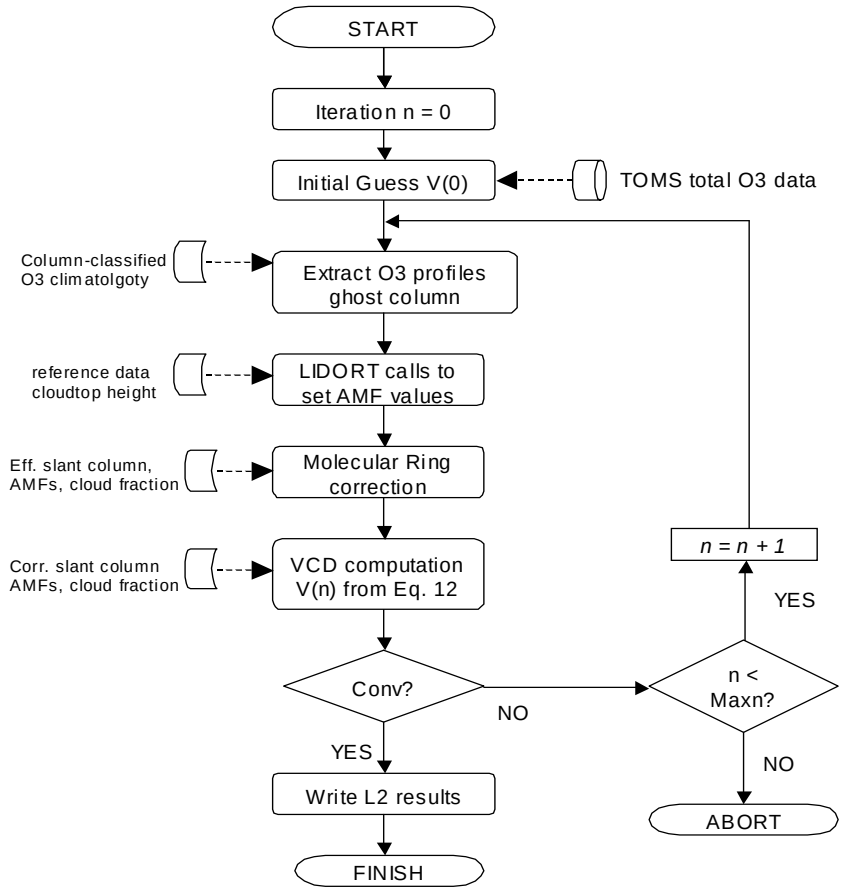

Figure 5. Functional diagram of the iterative solution scheme for O_3 AMFs and VCD.

However, the shape and total content of the selected ozone profile may bear little resemblance to the true profile, and (particularly for scenarios with high ozone content and/or high solar zenith angles) the AMF may then be incorrect due to a poor choice of input profile. The motivation behind the iterative approach is to circumvent this uncertainty by using information about the true profile to establish the AMF (and by extension, the vertical column density) more accurately. The only relevant profile information available to us in the DOAS context is the fitted slant column, and the iterative AMF/VCD algorithm uses the slant column result E to make an adjustment to the AMF (and hence the VCD) that reflects the trace gas content as expressed in the value of E. This adjustment depends on the use of an ozone profile climatology that is *column-classified* (in addition to other variables): for a given time and location, the choice of profile is then uniquely determined by the VCD. The use of such climatology is described in the next section.

In the ozone algorithm, there is now a molecular Ring correction M_{Ring} applied to the effective slant column E, and we must therefore use a corrected slant column $\mathrm{E_{corr}} = E/M_{\mathrm{Ring}}$ in the iteration. As we will see in the next section, M_{Ring} depends on the AMF, and hence M_{Ring} and $\mathrm{E_{corr}}$ will be updated for each new AMF computation

The iteration process is straightforward to describe; we treat first the clear-sky case. An initial AMF A_0 is computed given an initial choice V_0 of vertical column; the required profile

is drawn from the column-classified ensemble. The initial choice V_0 may be taken from the TOMS zonal mean column climatology, or (in the GOME operational context) from a previously retrieved result from an adjacent footprint. V_0 is the first guess for the iterated vertical column density. This value of A_0 is used to compute a Molecular Ring correction M_0. Given a slant column E from the DOAS fitting, we make the modified value $E_0 = E/M_0$. An updated vertical column V_1 is calculated through the relation $V_1 = E_0/A_0$. From the climatology, V_1 determines a new choice of profile, which is in turn used as input to a new AMF calculation, with result A_1. A new Ring factor M_1 and corrected slant column $E_1 = E/M_1$ is then calculated. The next guess V_2 for the vertical column follows from $V_2 = E_1/A_1$. This process is repeated until convergence has been reached (the relative difference between iterations of V is less than some small number).

For the partially cloudy footprint, the iteration proceeds via:

$$V^{(n+1)} = \frac{E^{(n)} + \Phi G^{(n)} A^{(n)}_{cloud}}{(1-\Phi)A^{(n)}_{clear} + \Phi A^{(n)}_{cloud}} \quad , \tag{7}$$

where the (n) superscript indicates the iteration number. In addition to the AMF results, the ghost column is also updated at each step. In this way, the ozone profile, the vertical column density, the ghost column density and both the AMFs have all been adjusted to fit the "true-situation" constraint imposed by the effective slant column. For the great majority of scenarios, convergence for ozone columns is rapid (3 or 4 iterations for a relative change of 0.1% in the vertical column).

This iterative AMF/VCD algorithm is straightforward to implement, and a flow diagram is shown in Figure 5. The DOAS-retrieved slant column E is a basic input; cloud auxiliary data is also required. Aside from the molecular Ring correction, the major difference between version 3.0 and the current GDP 4.0 is the use of the LIDORT RT model to generate AMFs “on-the-fly” (see box marked with a triple asterisk). In the earlier versions, a neural network ensemble replaces this box.

One of the advantages of “on-the-fly” computations is algorithm flexibility. Large multidimensional LUTs are cumbersome to manipulate and it takes time to create them from scratch (either for direct use or for off-line use in neural network training). There are no issues regarding the interpolation and extraction of look-up entries. In GDOAS it is straightforward to replace one reference data set or climatological profile with another without upsetting the modularity of the software.

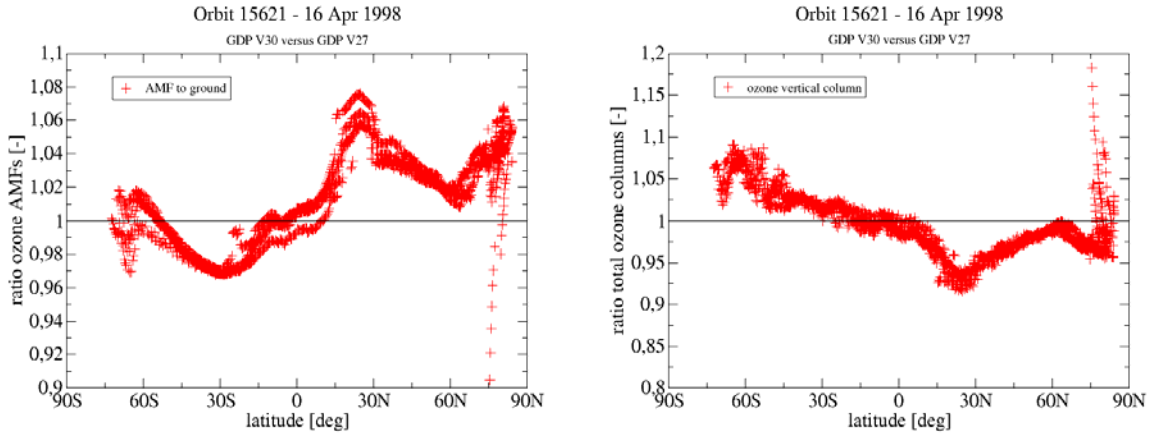

Figure 6. (Left) Ratios of clear sky AMFs from GDP 3.0 and 2.7 for a springtime GOME orbit. (Right) Vertical column densities.

We give one illustration of the improvements to be expected using an iterative AMF/VCD scheme (GDP Versions 3.0 and higher) as opposed to the single-profile AMF/VCD conversion used in the traditional DOAS algorithms (GDP 2.7 and earlier). Figure 6 (left) shows ratios of clear-sky AMFs (GDP 3.0 to 2.7) for a springtime orbit. The largest changes occur at mid and high northern latitudes, where GDP 3.0 AMFs are consistently higher, in agreement with the normally high ozone content at this time of year. In GDP 2.7, AMFs were too low because of inappropriate profile climatology choice. Jump artifacts at 20°N and 30°N are present in this algorithm due to the zonal classification used in the ozone climatology – such artifacts are absent in GDP 3.0 and 4.0. The corresponding vertical column densities are shown in the right-hand panel of Figure 6; southern mid-latitude differences are due mainly to the improved slant column fit (effective temperature fitting).

Of crucial importance in this scheme is the column-classified ozone profile climatology; the usage of such a data set is described in section 2.3.2 below. This is followed by a brief summary of the radiative transfer (RT) scattering model LIDORT as used in this application (section 2.3.3). A description of the neural network AMF training used in GDP 3.0 may be found in [Spurr et al., 2004]. A number of reference and climatology data sets (atmosphere temperature and pressure profiles, aerosol loadings and optical properties, Rayleigh scattering values, surface and cloud-top reflectance, ozone and other trace gas profiles) are required to create necessary inputs for the calls to the LIDORT model. These set-up operations are described in Section 2.3.4; we also note GDP 4.0 baseline settings for RT inputs.

2.3.2 Column-classified O_3 profile climatology

We require a way to assign a profile for a given choice of total column of ozone. Fortunately, this link was recognized a number of years ago by TOMS scientists at NASA, and the TOMS Version 7 [Wellemeyer et al., 1997] and Version 8 [Bhartia et al., 2003] column-classified ozone profile climatologies are well suited to this task.

In the TOMS Version 7 ("TV7") climatology, there are 26 profiles: 10 high- and 10 mid-latitude profiles with total columns of 125 DU to 575 DU at intervals of 50 DU, and 6 low

latitude profiles from 225 to 475 DU, also with a 50 DU increment. There are 11 "Umkehr" layers with pressure levels defined using scale heights; each partial column is given in DU. GDP 3.0 used this climatology. In order to avoid jump artifacts from one latitude zone to an adjacent zone, profiles from two zones are mixed using a distance-based weighting scheme.

The TV7 climatology was used in the original work with GDOAS in 2003. During preparations for the ITT Final Review at the end of 2003, it became clear that the new algorithms would benefit greatly from the use of the new TOMS Version 8 ("TV8") climatology, and NASA scientists kindly supplied this data in December 2003 [Bhartia et al., 2003]. The new TV8 data has a much more extensive classification, with 18 latitude zones at 10 degree intervals, 12 months of data, and variable numbers of columns (for example, tropical profiles typically require only 3 or 5 columns, whereas high-latitude profiles require a much greater range). Column amounts vary as before from 125 DU to 575 DU at 50 DU intervals. This new TV8 data set was used for the final GDOAS validation in January 2004, and is now the baseline for GDOAS in UPAS.

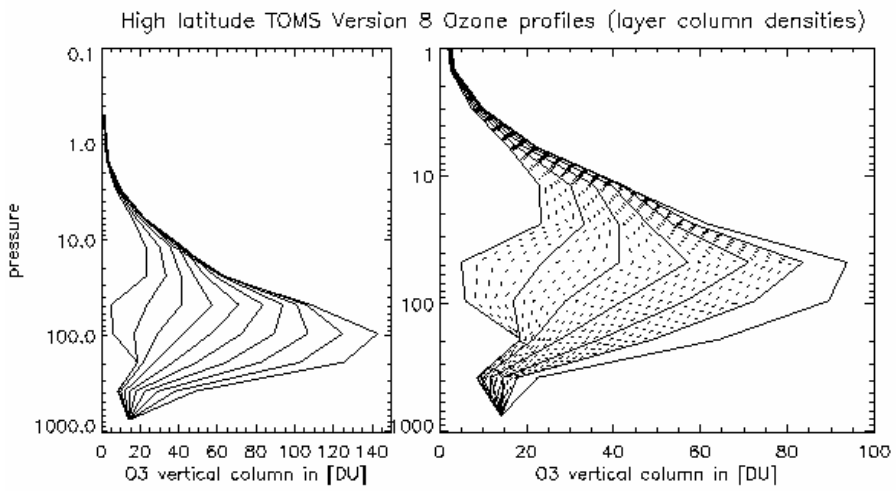

Figure 7. (Left) TOMS Version 8 high latitude profiles (partial column in [DU]. (Right) Intermediate profiles (dotted) for total columns at 10 DU intervals between data values.

To define a unique correspondence between profile and column, we proceed as follows. If the profile is defined by a set $\{U_j\}$ of partial columns, then the total column is $V = \sum_j U_j$. For two adjacent profiles $\{U_j^{(1)}\}$ and $\{U_j^{(2)}\}$ with total columns $V^{(1)}$ and $V^{(2)}$ we define an intermediate profile with column amount V according to:

$$U_j(V) = \left(\frac{V - V^{(1)}}{V^{(2)} - V^{(1)}}\right) U_j^{(2)} + \left(\frac{V^{(2)} - V}{V^{(2)} - V^{(1)}}\right) U_j^{(1)}. \qquad (8)$$

This defines a *linear* profile-column map. This map allows us to interpolate smoothly between profile entries in the climatology; the shape will vary continuously. We are drawing on an ensemble of possible profiles of which the climatology is a sample. If the vertical column lies outside the range of values classifying the climatology, we use spline extrapolation: this situation may occur in extreme ozone hole scenarios (total column <

125 DU). In Figure 7, we illustrate the application of this map for the set of 10 high-latitude TOMS profiles.

It is worth noting here that the simplest profile-column map is a scaling $U_j(V) = U_j^{(0)} V/V_0$ in terms of a fixed profile $U_j^{(0)}$ with column V_0. This mapping is implicit in traditional single-AMF DOAS retrieval algorithms. In this case, any profile associated with a retrieved total column will preserve the shape of the fixed profile (all layer partial columns are scaled equally). The assumption of a fixed ozone profile shape (with its typical stratospheric bulge) may generate sizeable AMF errors in (for instance) an ozone hole scenario.

The linear profile-column map determines the profile input required for radiative transfer. We note that these profiles are defined for a surface pressure of 1013 mb. For the clear sky profile, it will be necessary to adjust the lowest-layer partial column in line with the assigned surface pressure for a given GOME footprint. This is done by scaling the partial column with the logarithm of the layer pressure difference. For a cloudy-sky profile, the lowest layer is the one containing the cloud-top pressure as the lowest level, and the corresponding partial column will also scale with the logarithmic pressure drop. The ghost column is determined in [DU] by simple addition. In section 2.3.4 we will see how these important inputs are used to generate atmospheric optical property inputs required for the LIDORT scattering code.

2.3.3 LIDORT scattering code

In GDOAS we use the multiple scattering radiative transfer model code LIDORT [Spurr et al., 2001; Spurr, 2002] to simulate backscatter radiances needed for the AMFs. The atmosphere is assumed stratified, with a number of optically uniform sub-layers. LIDORT requires as input for each layer the total extinction optical thickness, the total layer single scatter albedos, and the total phase function scattering coefficients. All these quantities are constructed from knowledge of given atmospheric profiles of temperature, pressure, trace gas distributions, aerosol loading, plus knowledge of Rayleigh (molecular) scattering parameters, trace gas cross-sections, and aerosol optical properties. Like other discrete ordinate codes, LIDORT does not distinguish individual atmospheric distributions. The other major input is the surface reflection condition; in what follows we assume a Lambertian surface characterized by a total albedo, but BRDFs can be considered for sensitivity and error study.

The radiative transfer equation (RTE) for unpolarized light is

$$\mu \frac{\partial I(\Omega, x)}{\partial x} = I(\Omega, x) - \frac{\omega}{4\pi} \int P(\Omega, \Omega') I(\Omega', x) d\Omega' - \frac{\omega}{4\pi} P(\Omega, \Omega_0) F e^{-\alpha x}. \qquad (9)$$

Here $\Omega = \{\mu, \phi\}$, where μ is the cosine of the polar angle, ϕ is the azimuth angle between planes containing incident and scattering beams, and P is the phase function for scattering from direction Ω' to Ω. The first term in the source function is the multiple scatter contribution (diffuse radiation), and the second term is the primary scattering of direct sunlight of flux $F\mu_0$ at TOA. The solar direction is $\Omega_0 = \{-\mu_0, \phi_0\}$ at TOA; the factor α in the primary scatter attenuation is an average secant determined by ray-tracing through a spherical-shell atmosphere (the pseudo-spherical approximation). We use x for optical thickness.

The first step in the solution of Eq. (9) is the expansion of the diffuse field and the phase functions in terms of Fourier series in the cosine of the relative azimuth $\phi-\phi_0$. In the resulting equation for the Fourier component $I_m(x,\mu)$, the diffuse scatter polar-angle integral is replaced by a summation using a double Gauss-Legendre quadrature scheme. This results in a set of $2N$ coupled linear differential equations for the discrete ordinate intensities $I_m(\mu_j)$, where N is the number of quadrature streams in the half-space and $\{\mu_j, a_j\}$ ($j = \pm1 \ldots \pm N$) discrete ordinate polar directional cosines and quadrature weights. The equations are:

$$\mu \frac{\partial I_m(\mu_j)}{\partial x} = \pm I_m(\mu_j) - \frac{\omega}{2} \sum_{k=\pm1}^{\pm N} a_k P_m(\mu_j, \mu_k) I_m(\mu_k) - \frac{\omega}{2} P_m(\mu_j, -\mu_0) F e^{-\alpha x} . \qquad (10)$$

Here, P_m denotes the phase function appropriate to Fourier component m. The homogeneous equations in Eq. (10) are solved by standard eigenvalue methods, while the particular integral due to the primary scatter forcing is determined either by exponential substitution $I(\mu_j) \sim W(\mu_j) e^{-\alpha x}$ (see for example [Thomas and Stamnes, 1999], or by the more sophisticated Green's function methods [Siewert, 2000; Spurr, 2002]. Solutions for all layers are then fixed through the application of three boundary conditions: (1) no downwelling diffuse radiation at TOA; (2) a surface reflection condition at the lower boundary linking upwelling and downwelling intensities there; and (3) continuity of the radiation field at all intermediate layer boundaries. This results in a sparse linear matrix algebra problem $\mathbf{AX} = \mathbf{B}$ for the unknown vector of integration constants $\mathbf{X}$; solutions are found using standard numerical packages. This completes the discrete ordinate solution.

To obtain the field at arbitrary stream angle, we "post process" the solution by substituting the discrete ordinate solution in the original radiative transfer equation and integrating over partial and whole layer optical thickness values. This source function integration technique is tantamount to a smart interpolation of the discrete ordinate field. Summing the Fourier azimuth cosine series then completes the solution; an accuracy criterion is applied to this series to limit the number of Fourier terms to be calculated. For the TOA radiance, we have

$$I(0,\Omega) = I_{surf}(\mathrm{T}_n, \Omega) e^{-\mathrm{T}_n/\mu} + \sum_{p=1}^{n} \Lambda_p(\Omega) e^{-\mathrm{T}_p/\mu} , \qquad (11)$$

where Λ_p are the integrated layer source terms for layer p, $\exp(-\mathrm{T}_p/\mu)$ is the line-of-sight attenuation factor at cumulative optical depth T_p, and I_{surf} is the upwelling radiation at the bottom of the atmosphere (n layers; total optical thickness T_n). I_{surf} follows directly from the surface boundary condition. More details can be found in [Spurr, 2002].

Described here is the so-called pseudo-spherical (P-S) approximation, in which the solar beam attenuation is treated in a spherical shell atmosphere, but all scattering is still plane-parallel. This approximation is sufficiently accurate for solar zenith angles up to 90° and for line-of-sight viewing up to 30-35° from the nadir. A number of studies have shown that AMFs calculated with this assumption are sufficiently accurate for converting trace gas slant columns into vertical columns (see for example [Sarkissian et al., 1995]). However it should be noted that this AMF implementation is not sufficiently accurate for the polar-view mode of GOME, which is characterized by wide-angle off-nadir viewing. Here it is necessary to incorporate spherical corrections for line-of-sight paths as well as solar beams, and for this

we use the LIDORT Version 2.2+, which possesses this line-of-sight sphericity correction. In order to maintain consistency with the use of LIDORT in the polar view mode, it has been decided to use LIDORT V2.2+ for all calculations in GDP 4.0.

There are a number of practical issues associated with the on-line implementation of the LIDORT code in UPAS, and these are discussed in section 3.2.3 on algorithm verification.

2.3.4 Physical aspects for the RTM computation

Atmospheric distributions and surface quantities are required to calculate the optical property inputs required by LIDORT. This section describes the necessary physical steps in this process. In keeping with the flexibility and modularity of the GDOAS algorithm, the "atmospheric setup" function is decoupled from the LIDORT scattering code; it is straightforward to change input climatology without the need for lengthy reprocessing that is characteristic of LUT generation. The discussion here applies to the total ozone algorithm, with AMFs calculated at 325.5 nm; additional considerations appropriate to the total NO_2 algorithm are noted below in section 2.5.2. For ozone AMFs, the operational baseline for GDOAS/GDP 4.0 is to avoid the use of aerosols in the RTM computation.

Pressure and temperature

In the GDOAS baseline, the TOMS V7 and V8 pressure levels set the atmospheric layering; pressures are halved for each successive atmospheric boundary. There are 14 levels in all, Top-of-atmosphere (TOA) is set at 0.03 hPa, and surface pressure is allowed to vary. Temperature profiles are required for hydrostatic balance and the determination of ozone cross sections. Temperatures are interpolated (where appropriate) to the pressure grid (linearly with log-pressure). Height levels (required for the average secant factors in the solar beam attenuation) are determined by hydrostatic equilibrium based on a reference height input (the surface topographical height). The acceleration due to gravity is allowed to vary with latitude and height according to the specification in [Bodhaine et al., 1999]. As noted above in section 2.3.3, the lowest layer adjusted to fit the boundary pressure (surface or cloud-top).

A temperature profile must be taken from external data sources. [For GDP 3.0, TOMS V7 temperature profiles were used without interpolation]. For TOMS V8 (the UPAS/GDOAS default), we use a latitude-zone monthly temperature climatology supplied with the ozone profiles.

We assign a surface height and surface pressure for each GOME footprint. The default is the GTOP30 topographical database for surface height; this replaces the GTOP05 data set used in previous GDP versions. Surface pressure may be established from surface height by interpolation.

Molecular Scattering and Extinction

As noted already in the DOAS fitting description, O_3 and NO_2 cross sections are taken from the GOME FM 98 data set; the baseline uses pre-shifted data. The same cross-sections are used in the radiative transfer set-up. Though NO_2 is included in the ozone DOAS fitting, it is ignored in the ozone AMF calculations.

Rayleigh scattering $\sigma^{Ray}(\lambda)$ will be determined from a standard formula, but using the latest parameterizations as given in [Bodhaine et al., 1999]. Layer air column density D_p in layer p depends only on the pressure difference across the layer (in hydrostatic equilibrium). However we again allow for height variations of gravity in the computation of D_p.

In terms of the ozone partial columns U_p in layer p, the extinction optical thickness and single scatter albedo are:

$$\delta_p = \sigma^{Ray}(\lambda) D_p + \sigma_p^{O3}(\lambda) U_p \quad ; \quad \omega_p = \frac{\sigma^{Ray}(\lambda) D_p}{\delta_p} ; \tag{13}$$

For molecular (Rayleigh) scattering, the phase function has a $cos^2\Theta$ dependence on scattering angle Θ, with only two non-vanishing Legendre polynomial expansion coefficients $\beta_0 = 1$, $\beta_2 = (1 + \rho) / (2 + \rho)$, where the depolarization ratio ρ is taken from [Chance and Spurr, 1997].

Surface data

The static surface albedo climatology used in earlier versions [Matthews, 1983; Bowker et al., 1985] was found to be unrepresentative in some regions, particularly at higher latitudes. It is better to use dynamic albedo data sets derived from accumulated satellite reflectance data. In GDP 4.0, we use a combination of the GOME Lambertian equivalent reflectivity (LER) data set of albedos prepared from 5.5 years of GOME reflectivity data [Koelemeijer et al., 2003], and the Nimbus-7 TOMS LER data set prepared from 14.5 years of data from 1978 onwards [Herman and Celarier, 1997], and valid for 340 to 380 nm. The GOME LER data has monthly and yearly entries on a 1°-1° latitude/longitude grid, at 12 different wavelengths spanning the GOME range; the TOMS data is also monthly. We use GOME LER data at 335 and 380 nm, and TOMS LER data at 380 nm; the desired combination albedo is $a(\lambda) = s(\lambda) a_{TOMS}(380)$, where the scaling is $s(\lambda) = a_{GOME}(\lambda)/a_{GOME}(380)$, and λ = 335 nm for total ozone fitting [Boersma et al., 2004].

In Figure 8 we show the effect of this database change on the total ozone columns for four orbits. These results were obtained using GOME LER data, $a(\lambda) = a_{GOME}(335)$; results for the combination albedo are similar. Note in particular the reduced columns at high northern latitudes in winter (red) and spring (blue) due to the greater sensitivity to sea ice in the GOME LER data set.

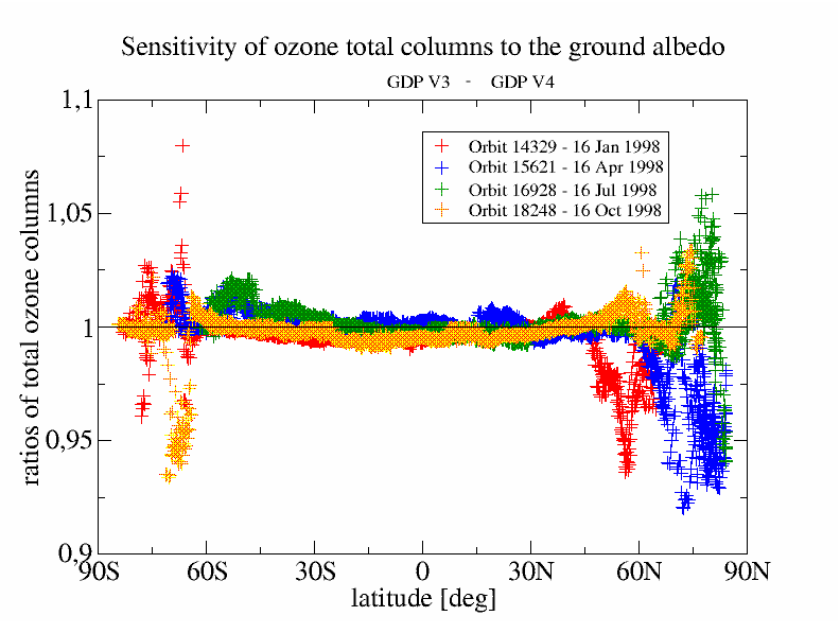

Figure 8. Ozone column differences for the old (GDP 3.0) and new albedo databases (GDP 4.0, GOME LER data only). Results are shown for four orbits.

Aerosols

There is very little information on aerosols to be gleaned from column ozone retrieval in the UV (absorbing aerosols can be detected, but it is difficult to derive their optical properties). As noted already, the operational default is to avoid the use of aerosols in the GDOAS/GDP 4.0 ozone AMF computations. AMF and VCD iterations are insensitive to the choice of aerosol, and this sensitivity issue has been examined for selected orbits as part of the GDOAS review work (see section 3.5). Aerosol information is required for these GDOAS AMF sensitivity issues, and we have taken the MODTRAN aerosol data sets [Kneizys et al., 1988; Berk et al., 1989] as a reference; these provide aerosol loading and optical properties. All aerosol inputs are linearly interpolated to the clear sky and cloudy sky height grids; aerosol scattering distributions were assumed to follow the Henyey-Greenstein phase function law.

Cloud issues

Clouds are treated in the independent pixel approximation (IPA), in which TOA radiance in a partially cloudy scenario is simulated as a linear combination of backscatter from clear and fully cloudy scenes, weighted by an effective cloud fractional cover f_c. In RT simulations for the AMFs, clouds are regarded as highly reflecting Lambertian surfaces. Atmospheric profiles are prepared for both the clear and cloudy sky scenarios. For layers not including but above the immediate cloud-top layer, atmospheric properties can be copied from the clear sky profiles. The "ghost column" calculation is straightforward in GDOAS, once the profile/column mapping is known. In this IPA treatment, cloud information is condensed to a small set of 3 parameters (cloud fraction, cloud-top albedo and cloud-top pressure).

UPAS/GDOAS represents a new departure for cloud pre-processing: we no longer use the ICFA algorithm that featured in all previous versions of GDP. UPAS/GDOAS has two options for cloud pre-processing (the OCRA/ROCINN and FRESCO algorithms). The GDP

4.0 operational baseline uses the OCRA/ROCINN combination - a cloud property algorithm at DLR installed recently in UPAS as a pre-processing step to be executed before total column retrieval. OCRA [Loyola, 1998b; Loyola, 2000] is a data fusion algorithm based on GOME sub-pixel PMD output; it delivers an effective cloud fraction. ROCINN [Loyola, 2004] is a new algorithm based on O_2 *A*-band reflectivities from GOME; ROCINN delivers cloud-top pressure and cloud-top albedo; both of which will be used in RT simulations. The algorithms are summarized in section 2.6. Based on recent validation results [Tuinder et al., 2004; Loyola 2004], we believe that the OCRA/ROCINN combination is currently the best choice for the cloud product baseline for GDP 4.0.

UPAS/GDOAS can also ingest results from the FRESCO O_2 *A* Band algorithm [Koelemeijer et al., 2001] (fitted values of f_c and effective cloud-top pressure p_c, plus errors). FRESCO itself is not part of GDP. FRESCO data was used in the verification phase, and in the validation phase, data was prepared off-line for a subset of delta validation orbits.

Polarization issues

In ozone profile retrievals, the polarization correction applied to Level 1 data is an important source of error; the inclusion of polarization in the RT simulations is also an important consideration for the profile algorithm [van Oss et al., 2001]. However, in a DOAS fitting with narrow windows in the range 325-335 nm, the polarization signature is subsumed in the low-filter polynomial; polarization is neglected in AMF RT calculations.

2.4 Molecular Ring effect correction

2.4.1 Introduction

As noted already, DOAS retrieval in GDP 3.0 neglects the contribution of the so-called telluric (molecular) Ring effect. The spectral dependence in this molecular Ring effect correlates quite strongly with the behavior of the ozone absorption. In closed-loop tests using synthetic radiances created using a radiative transfer model including first-order rotational Raman scattering [Vountas et al., 1998], it was found that neglect of the telluric Ring effect leads to systematic underestimation of ozone total columns (up to 10%) [van Roozendael et al., 2002]. A correction for the molecular Ring effect in ozone retrieval was developed during the GOME geophysical validation campaign in 2002 ([van Roozendael et al., 2002]. A full description of this correction, including error analysis, will be provided in a forthcoming paper [van Roozendael et al., 2004]. Here the principle of the method and main equations are given, together with an example of its implementation in the GDP system. We also include a short note on closed-loop testing of this algorithm component.

Considering only O_3 absorption, the correction is based on a simplified forward model of the intensity at satellite *I(λ)* which includes an explicit contribution due to inelastic rotational Raman scattering (RRS):

$$I(\lambda) = I^0(\lambda) \cdot \exp\left[-\sigma_{O3}(\lambda) \cdot E_{O3} - P_1^{\lambda}\right] + E_{Ring} \cdot I_0^{RRS}(\lambda) \cdot \exp\left[-\sigma_{O3}(\lambda) \cdot E_{O3}^{RRS} - P_2^{\lambda}\right]. \qquad (14)$$

The first term on the right-hand side describes elastic scattering and follows directly from the Lambert-Beer law, with $I^0(\lambda)$ the solar intensity, P_λ a low-order polynomial, and σ_{O3} and E_{O3} the ozone absorption cross-section and effective slant column respectively.

The Ring effect is modeled by the second term. We may consider several approximations. First, the Raman light is assumed to be produced close to the surface, with a spectral shape given by a source spectrum for Raman scattering $I_0^{RRS}(\lambda)$. This source spectrum only treats the spectral smoothing effect of RRS on the solar intensity. In practice it is calculated by convolution of a GOME irradiance spectrum using rotational Raman cross sections appropriate to inelastic scattering into the wavelength of interest. The fractional intensity of Raman light (the E_{Ring} parameter) is freely adjustable; this may vary considerably and will depend on parameters such as cloud coverage, cloud altitude and surface albedo. Ozone absorption (the term $\sigma_{O3}(\lambda).E_{O3}^{RRS}$) is then treated consistently, assuming that Raman photons produced at the surface and/or above clouds travel upward to the satellite. Ozone absorption taking place in the incoming light is assumed to be fully smeared out in the inelastic process, so that it can be neglected in first approximation.

2.4.2 DOAS implementation

In order to allow implementation in a linearized DOAS formalism, equation (14) can be rewritten (after a Taylor expansion of small terms) in the following way:

$$\ln\left[\frac{I(\lambda)}{I^0(\lambda)}\right] = -\sigma_{O3}(\lambda).E'_{O3} - \sigma_{Ring}(\lambda).E_{Ring} - P(\lambda), \tag{15}$$

with the Ring cross-section $\sigma_{Ring}(\lambda)$ defined as:

$$\sigma_{Ring}(\lambda) = -\frac{I_0^{RRS}(\lambda)}{I^0(\lambda)}. \tag{16}$$

Equation (15) is the familiar DOAS forward-model law, from which E'_{O3}, E_{Ring} and polynomial coefficients can be determined in the usual manner. The major difference with Ring correction methods used in previous studies comes in the definition of the modified O_3 effective slant column E'_{O3}, which is related to the effective slant column for *elastic* scattering (E_{O3}) by the following formula:

$$E'_{O3} \cong E_{O3}.\left\{1 + E_{Ring}\cdot\overline{\sigma}_{Ring}\cdot\left(1 - \frac{\sec(\theta_0)}{A_{total}}\right)\right\} = E_{O3}.M_{Ring}, \tag{17}$$

where A_{O3} is the ozone AMF, θ_0 the solar zenith angle, and $\overline{\sigma}_{Ring}$ an average Ring cross-section calculated over the spectral fitting interval. For cloudy situations, appropriate weighting under the independent pixel approximation can be obtained using the standard definition of the total AMF: $A_{total} = (1-\Phi)A_{clear} + \Phi A_{cloud}$, where Φ is the effective cloud fraction or intensity-weighted cloud fraction, and A_{clear} and A_{cloud} the clear-sky and cloudy AMFs.

In this formulation, the DOAS fitting is essentially unchanged; it gives fitted parameters E'_{O3} and E_{Ring}. The effective slant column for ozone is then adjusted *after* the fit through the

relation $E_{O3} = M_{Ring}\, E'_{O3}$. Note that the molecular Ring term M_{Ring} can also be used to quantify the error due to an incorrect estimation of the Ring effect in previous GDP versions.

Eq. (17) defines the Ring correction; the definition requires knowledge of AMFs. Studies have shown that for moderate solar zenith angles, the geometrical AMF is sufficiently accurate to approximate A_{total}. For high solar zenith angles with long paths through absorbing ozone layers, a more precise calculation is needed. In GDOAS, we use the total AMF already computed at each AMF/VCD iteration step – thus the molecular Ring correction must also be applied at each iteration to the DOAS slant column result before a new estimate is made for the VCD.

2.4.3 Discussion; example

Figure 9 shows values of the molecular Ring correction term M_{Ring} for four seasonally representative GOME orbits. Ozone effective slant columns are clearly scaled up by 2-9% and this is more than enough to compensate for the negative bias observed in several GOME validation campaigns for GDP 3.0.

The general shape of the correction factor is due to the variation of the solar zenith angle along the GOME orbit. Pronounced peaks and high-frequency oscillations are mainly due to clouds, but changes of surface albedo and surface height also influence this factor. The cloud impact is especially visible for orbit 18248 (orange) at latitudes of 10°N and 30°S where the GOME measurements were affected by high clouds and the high cloud fractional cover typically found in tropical regions. The influence of the surface albedo is obvious at high Southern latitudes where a sharp increase of the albedo around 60°S due to sea ice and the Antarctic ice shield is associated with a corresponding decrease of the Ring correction term.

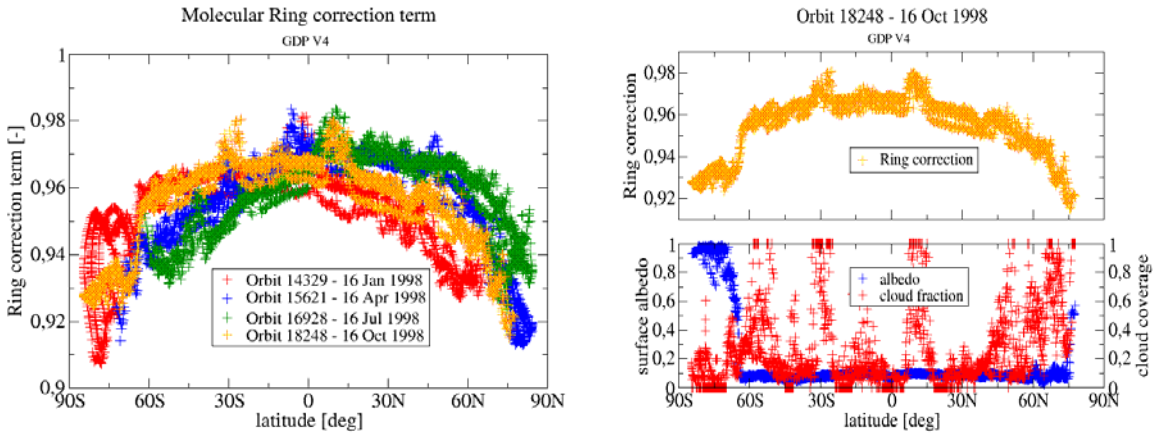

Figure 9. Molecular Ring correction factors for four GOME orbits in 1998 (left panel) and Ring correction, surface albedo and fractional cloud cover for one GOME Orbit (right panel). See text for more information.

2.4.4 Closed-loop testing

We conclude this section with a short summary of the radiative transfer simulations required for the closed-loop testing of the new Ring effect implementation. RRS correction factors are defined as relative differences between backscatter radiances calculated with and without RRS. The models used are the SCIATRAN code in a version with first-order RRS implementation [Vountas et al., 1998], and the more recent LIDORT-RRS discrete ordinate model [Spurr, 2004]. Both models are first order in RRS; that is, in addition to the primary inelastic RRS of the solar beam, diffuse source terms for radiation that is Raman scattered into a wavelength λ are computed using the zero-order (elastic) radiation field at wavelengths corresponding to the Raman energy levels.

The first closed-loop tests of the new Ring implementation were done using the SCIATRAN model to compute synthetic radiances for a wavelength range 320-340 nm, with ozone climatological profiles [Fortuin and Kelder, 1999] and associated ECMWF temperature data, and for a representative range of solar viewing conditions. Retrievals were done using an older traditional DOAS method (for details, see [van Roozendael et al., 2002]).

For the GDOAS algorithm, a more extensive LUT of Ring correction factors has been generated using the LIDORT-RRS model. Discrete ordinate solutions in LIDORT-RRS are entirely analytic, and the model is able to generate output at arbitrary viewing geometry and optical depth. The LUT is classified as follows; by solar zenith angle (20 values from 15 to 88°), by line-of-sight zenith angle (4 values: 0, 10, 20, 31°), by relative azimuth angle (5 values from 0 to 180°), by albedos (7 values: 0.0, 0.05, 0.1, 0.2, 0.5, 0.8, 1.0), by ozone profiles (26 TOMS V7 profiles [Wellemeyer et al., 1997]), and by lower boundary pressure (11 values from 1050 hPa to 100 hPa). This takes care of all geophysical clear sky and cloud-filled scenarios.

All calculations were done in a Rayleigh atmosphere (no aerosols). Although solar zenith angle and albedo are the major dependencies, lower boundary pressure is important because the bulk of inelastic scattering takes place in the lower troposphere. Ring corrections were computed at 220 wavelength points between 315 and 335 nm, using a GOME solar spectrum at resolution of approximately 0.105 nm. Interpolation from the LUT is done linearly (table entries are dense enough). The table takes 1 day to create. Results from the closed-loop analyses are described in detail in the GODFIT/GDOAS Validation Report [R1, R2].

2.5 NO_2 total column algorithm

2.5.1 Summary

The ESA ITT studies were concerned with the development of improved total ozone algorithms, and the major emphasis from an operational viewpoint has been the reprocessing of the total ozone record. However, the NO_2 total column is part of the GOME Level 2 product and it is a requirement to perform a simultaneous reprocessing of the NO_2 record. Due to time and budget limitations, a necessarily limited set of improvements has been implemented in GDP 4.0, and these are discussed below. Research on NO_2 column retrieval (in particular the division into tropospheric and stratospheric columns) is currently an active area, and it is anticipated that code improvements (based on recent research results and new

methods) will be established in the operational GDP framework in the future, both for GOME and the upcoming GOME-2 algorithms.

2.5.2 DOAS NO_2 slant column fitting

The DOAS slant-column fitting procedure for NO_2 has changed little from GDP 2.7 and GDP 3.0 to 4.0; the main change is an upgrade of various reference spectra. The GDP 2.7 NO_2 spectral fitting has been compared successfully with other DOAS algorithms using GOME data [Boersma et al., 2004]. The GDP 4.0 NO_2 DOAS algorithm is very similar to that for total ozone, and uses the same least squares fitting package implemented in UPAS; the description in Section 2.2 is relevant here, with the following differences:

1) The fitting window is 425-450 nm in GOME Channel 3. NO_2 absorption features are prominent, and GOME measurements have high signal-to-noise and manageable interference effects.
2) A single NO_2 cross-section reference spectrum is used. This is the GOME FM Channel 3 cross-section at 241 K [Burrows et al., 1998b]. There is no retrieval of an effective temperature; temperature dependence of the cross-sections is ignored.
3) There are two additive undersampling spectra and one additive Fraunhofer Ring spectrum for this region of GOME Channel 3; new undersampling spectra have been prepared at BIRA-IASB, as well as an updated Fraunhofer spectrum.
4) Intensity offset effects that may be induced by residual stray-light or imperfect Level 0-1 processing are known to be sources of bias in DOAS retrievals of minor trace species; to correct for offset the inverse of the sun spectrum is fitted as another effective cross-section.
5) O_3 is an interfering species and the slant column amplitude for it is included in the fit. However, O_3 absorption in this part of the Chappuis bands is weak (one reason for the fitting window choice). GOME FM98 data at 221 K are used [Burrows et al., 1999a].
6) O_2-O_2 and H_2O are interfering species and slant column amplitudes for them are included in the fit. Sources are [Greenblatt et al., 1990] for O_2-O_2 (recalibrated) and HITRAN [Rothman et al., 2003] for H_2O (the latter as input to line-by-line computations which are followed by slit function convolution).
7) There is no molecular Ring correction implemented.

The total number of fitting parameters is 12, comprising 4 trace gas slant columns, 4 polynomial coefficients, and 4 amplitudes for additive reference spectra. Wavelength registration is done as for total ozone DOAS: the solar spectrum is the wavelength standard, with a shift-and-squeeze fitting performed for each footprint for resampling the earthshine spectrum. “Post Level 1” wavelength registration for the solar spectrum is improved at the orbit start by an additional cross-correlation covering the 425-450 nm fitting window.

Diffuser plate sensitivity in this region of the GOME solar spectrum is significant, and can lead to artifacts. It is difficult to characterize consistently for the length of the GOME data record, and attempts to do so may be summarized as follows:

1. A single solar reference spectrum can be used in the DOAS fit. This approach can be used for processing a limited period of GOME data (e.g. 1-3 years) [Wenig et al.,

2004], However, due to degradation of the GOME instrument, this approach is not applicable for processing the entire 9-year record.

2. Solar reference spectra can be changed regularly, based on specific information derived from a post-processing operation involving renormalization in "stable" NO_2 regions (over the oceans). This is an *ex post facto* operation that has to done on a daily basis; it will not be feasible for the GDP 4.0 reprocessing. Attempts are currently underway to correct for the whole data set in this manner.
3. Probably, the best solution is to reprocess the entire GOME Level-1 data set, based on better parameterizations of BRDF spectral features from an examination of GOME irradiance data. This relative correction method is under development [Slijkhuis, 2004].

Given the extremely limited time and resources for this reprocessing and the experimental status of these methods,, the GDP 4.0 baseline at this point will be to use solar spectra without accounting for this sensitivity.

2.5.3 AMF and VCD determination

NO_2 AMF calculations in GDP 3.0 and earlier versions have been based on exact single-scatter AMF calculations, with multiple scatter corrections from look-up tables. AMF calculations have been based on a single NO_2 profile from the USA standard atmosphere. As noted above, clear and cloudy-sky AMFs are combined assuming the IPA, and the VCD calculation follows the usual formula. There is no AMF/VCD iteration. AMFs are not sensitive to wavelength, and it is usual to choose the window mid-point (437.5 nm).

The issue of NO_2 AMFs is currently an area of active research [Leue et al., 2001; Richter and Burrows, 2002; Martin et al., 2002; Boersma et al., 2004; Wenig et al., 2004].

In the short term for GDP 4.0, we adopt the following baseline. Given that GDP 4.0 has already an on-the-fly AMF capability based on calls to the LIDORT model, we will adapt the code developed for the total ozone algorithm, and calculate AMFs in this manner for the NO_2 problem. To incorporate the seasonal and latitudinal variation in stratospheric NO_2 in the AMF calculations, a composite climatology of stratospheric NO_2 profiles from Lambert and Granville [2004] is used. It will not be possible in the short term to ingest any kind of tropospheric profile from chemical model output and perform the requisite (time-consuming) sensitivity analysis, so the baseline for the AMF calculations will be the absence of NO_2 in the troposphere.

With this choice of profiles, the vertical resolution need not be too fine, and it will be sufficient to use the 13-layer grid based on TOMS pressure levels that was used for the ozone AMF computations. Molecular scattering and aerosol optical properties will again be drawn from the sources mentioned in section 2.3.4. Ozone profiles will be taken from the TOMS climatology (this is not a critical consideration). Cloud information will be used in the same way as before. The choice of surface albedo will again be combined from the GOME LER (values at 380 nm and 440 nm) and TOMS LER (values at 380 nm) databases.

2.6 Cloud algorithm summaries

2.6.1 OCRA

The basic idea in OCRA (Optical Cloud Recognition Algorithm [Loyola and Ruppert, 1998b]) is to decompose optical sensor measurements into two components: a cloud-free background and a remainder expressing the influence of clouds. The key to the algorithm is the construction of the cloud-free composite that is invariant with respect to the atmosphere, and to topography and solar and viewing angles. Some pre-processing is required before multi-temporal data can be fused to develop the composite.

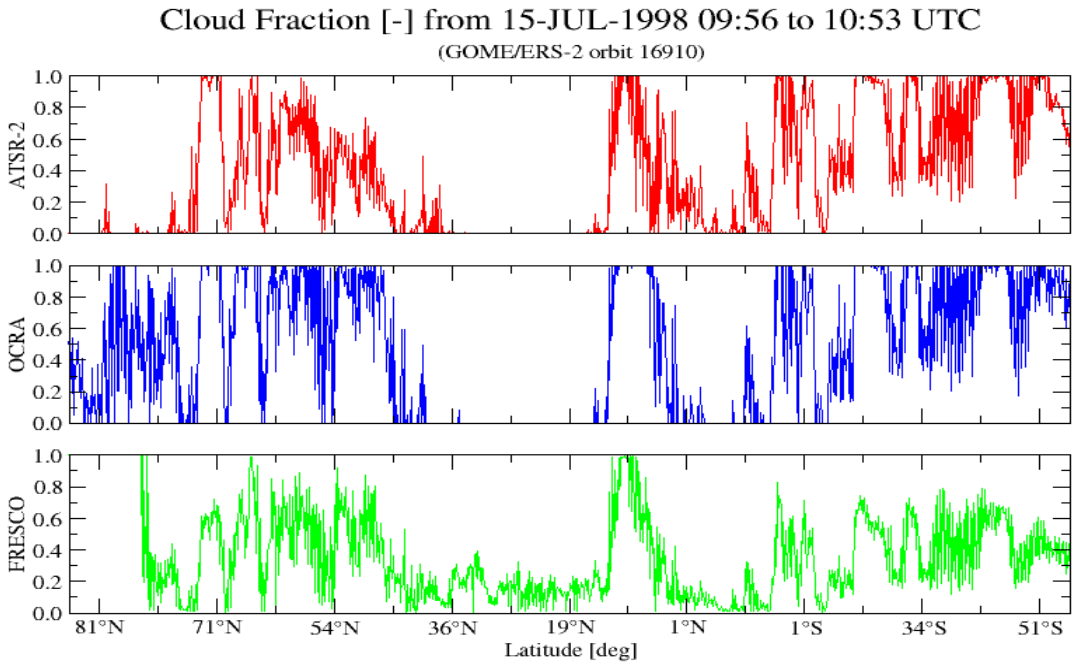

Figure 10. Comparison of cloud fraction retrieved from GOME using the OCRA algorithm (middle panel), the FRESCO algorithm (lower panel) and the ATSR-2 sensor (upper panel).

For a given location (x,y), we define a reflectance factor $\rho(x,y,\lambda)$ at wavelength λ for the ground cover projection of the image via the relation

$$\rho(x,y,\lambda) = \frac{I(x,y,\lambda)}{I_0(\lambda)\cos(\theta_0)\cos(\theta)}, \tag{18}$$

where I is the upwelling radiance into the satellite, I_0 is the solar irradiance, and θ_0 and θ the solar and viewing zenith angles respectively. This reflectance is translated into normalized *rg*-color space via

$$r = \frac{\rho(x,y,\lambda_R)}{\sum_{i=R,G,B}\rho(x,y,\lambda_i)}, g = \frac{\rho(x,y,\lambda_G)}{\sum_{i=R,G,B}\rho(x,y,\lambda_i)}. \tag{19}$$

If we have a set M = of *n* normalized multi-temporal measurements over the same location (*x*,*y*), then a cloud-free (or minimum cloudiness) pixel rg_{CF} in M is selected with the brightness criterion $\|rg_{CF} - w\| \geq \|rg_k - w\|$ for $k = 1,..,n$, where $w = (1/3,1/3)$ is the *white point* in the *rg* chromaticity diagram. A global cloud-free composite is then constructed by merging cloud-free reflectances $\rho_{CF}(\lambda)$ (corresponding to rg_{CF}) at all locations. The effective cloud fraction is then determined by examining separations between RGB reflectances and their cloud-free composite values:

$$f = \sqrt{\sum_{i=R,G,B_i} \alpha(\lambda_i) \max(0, [\rho(\lambda_i) - \rho_{CF}(\lambda_i)]^2 - \beta(\lambda_i))} \,. \tag{20}$$

Scaling factors α ensure that the cloud fraction is mapped to the interval [0,1], while offsets β account for aerosol and other radiative effects in the atmosphere. A detailed description of the algorithm and its application to satellite data is given in [Loyola, 2000].

OCRA was validated by comparing effective cloud fractions to values derived from collocated measurements from the ATSR-2 instrument (also on board ERS-2). The cloud fraction determined with OCRA, FRESCO [Koelemeijer and Stammes, 2001] and ATSR-2 in July 15th 1998 is shown in Figure 10. In general, OCRA results are close to those for ATSR-2, while FRESCO has a tendency to underestimate the cloud fraction. OCRA performs well also over desert and snow/ice conditions, while FRESCO has problems over desert regions (e.g. between 35°N to 20°N in Figure 10). This ATSR-2 comparison confirms the results reported in [Tuinder et al., 2004] where several algorithms for retrieving cloud fraction using GOME data where compared against synoptic surface observations: in this work, OCRA has a mean difference of only −10% compared with synoptic data, followed by FRESCO (−19.7%) and ICFA (−38.9%).

2.6.2 ROCINN

ROCINN [Loyola, 2004] is a new algorithm based on O_2 *A*-band reflectances from GOME: it will deliver cloud-top pressure and cloud-top albedo; the cloud fraction is assumed known (from OCRA). The impact of the OCRA/ROCINN algorithm on retrieved total ozone columns was assessed in the verification phase for a carefully selected subset of validation orbits (which included ozone hole scenarios).

In the IPA treatment, the total reflectivity is assumed to be a weighted sum of independent reflectivities from the surface and cloud-top, the weighting expressed through the effective cloud fraction f_c. In the forward model simulations, only attenuation through oxygen absorption of the direct solar beam and its reflection from ground or cloud-top is considered in the radiative transfer. Molecular scattering, scattering and absorption by aerosols and diffuse surface reflection are neglected, as is absorption by oxygen within and below any clouds. Surfaces are assumed to be Lambertian reflectors. In this approximation, we need only consider transmittances along two photon paths through the atmosphere, and the forward model reflectivity simulation is then:

$$R_{sim}(\lambda) = f_c A_c \langle T(\lambda, \Theta, z_c) \rangle + (1 - f_c) A_s \langle T(\lambda, \Theta, z_s) \rangle \tag{21}$$

Here, $\langle T \rangle$ denotes the convoluted transmittance to surface or cloud-top for path geometry Θ (solar zenith angle and line-of-sight angle), wavelength λ and lower boundary heights z_s (surface) and z_c (cloud-top). Line-by-line transmittances must first be calculated using line spectroscopic information for the O_2 *A*-band (taken from the HITRAN database [Rothman et al., 2003]), before convolution with the GOME slit function. The values z_s, A_s (surface albedo, taken from a suitable database) are assumed known. Cloud fraction f_c is taken from the OCRA result, and ROCINN aims to retrieve z_c and the cloud-top albedo A_c.

RT calculations based on Eq. (21) are used to create a complete data set of simulated reflectances for all viewing geometries and geophysical scenarios, for various combinations of cloud fraction, cloud-top height and cloud-top albedo. High-resolution transmittances are computed for the range 758-772 nm at resolution 0.01 nm before convolution.

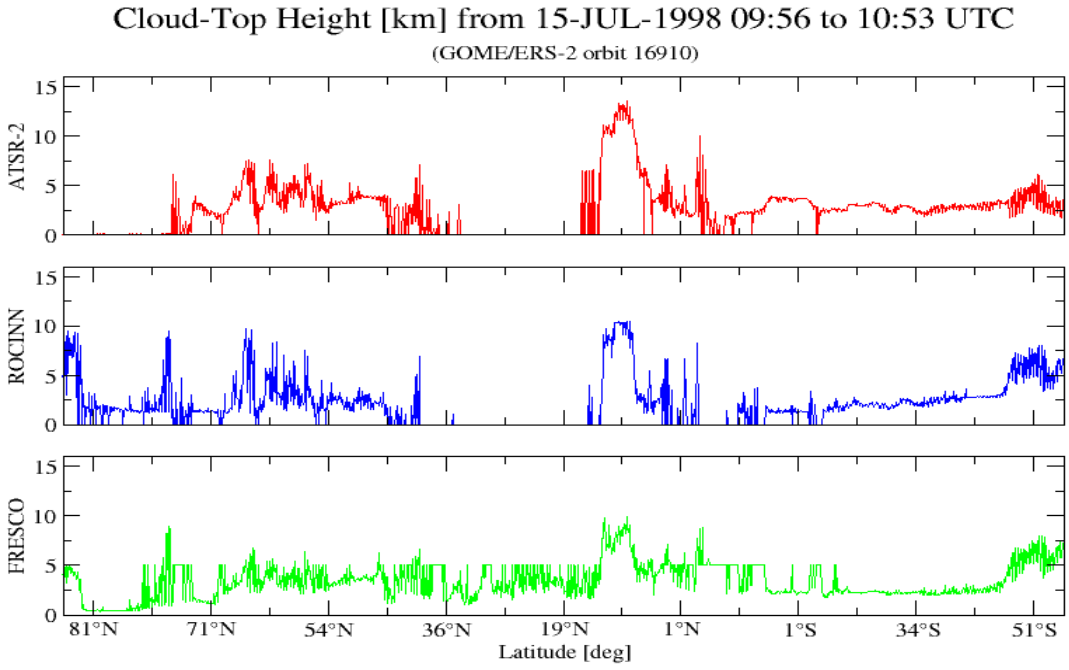

Figure 11. Comparison of cloud-top height retrieved from GOME using the ROCINN algorithm (middle panel), the FRESCO algorithm (lower panel) and the ATSR-2 sensor (upper panel).

In ROCINN, the forward model function computing reflectance is represented by the data set $S = \{(X_i, Y_i)\}$ for $i = 1,\ldots,s$. Inputs X are the parameters $\{f_c, \Theta, A_s, z_s, A_c, z_c\}$. The output Y are the simulated radiances $\{R_{sim}(\lambda)\}$. To generate an inverse data set, we first add normal distributed Gaussian measurement noise ε to the simulated radiances: $R = R_{sim} + \varepsilon$.

We may now generate the inverse data set $S^* = \{(X_i^*, Y_i^*)\}$ for $i = 1,\ldots,s$, where now the input set X^* comprises the parameters $\{R_{sim}(\lambda), f_c, \Theta, A_s, z_s\}$ and the output is now $Y^* = \{A_c, z_c\}$, the unknown cloud-top albedo and cloud-top height. A neural network NN_{INV} is finally trained with the *inverse* data set S^*, giving the result:

$$\{A_c, z_c\} = NN_{INV}(R_{sim}(\lambda), f_c, \Theta, A_s, z_s) \quad (22)$$

For more details on the use of neural networks to solve inverse problems, see [Loyola, 2004].

Cloud-top heights determined with ROCINN, FRESCO and ATSR-2 for a July 15th 1998 orbit are shown in Figure 11. The three algorithms provide similar results; ROCINN is smoother and more stable than FRESCO and has fewer spikes. ROCINN computes realistic cloud-top height values even for pixels with a low cloud fraction (e.g. around 1°S), what is not the case for FRESCO that reports a default fix value of 5 km for pixels with cloud fraction < 0.1. ROCINN does not produce outliers probably because the neural network is more robust and it finds a global minimal solution to the inverse function, while FRESCO finds a local minimal solution for each single measurement. Note that for cloud-free scenes (e.g. between 35°N to 20°N) both ATSR-2 and ROCINN report a cloud-top height of zero, while FRESCO retrieves the effective ground surface height.

2.7 Errors in the total ozone algorithm

2.7.1 Error propagation

To recap, the conversion to vertical column V proceeds via the relation (see Section 2.3.1):

$$V = \frac{E + \Phi G A_{cloud}}{A_T} \quad , \qquad \text{where} \quad A_T = (1-\Phi)A_{clear} + \Phi A_{cloud} \, .$$

The error on V (which we denote as s_V) can be expressed as a function of the error on component parameters E (ozone slant column), G (ghost vertical column),Φ (cloud fraction or radiance-weighted cloud fraction), A_{clear} (AMF to ground or clear sky), A_{cloud} (AMF to cloud-top). A complete definition of the error on V can be derived from error propagation rules:

$$s_V^2 = \left(\frac{\partial V}{\partial E}\right)^2 \cdot s_E^2 + \left(\frac{\partial V}{\partial A_{clear}}\right)^2 \cdot s_{A_{clear}}^2 + \left(\frac{\partial V}{\partial A_{cloud}}\right)^2 \cdot s_{A_{cloud}}^2 + \left(\frac{\partial V}{\partial \Phi}\right)^2 \cdot s_\Phi^2 + \left(\frac{\partial V}{\partial G}\right)^2 \cdot s_G^2$$

From the definition of V, we find:

$$\frac{\partial V}{\partial E} = \frac{1}{A_T}; \qquad \frac{\partial V}{\partial G} = \Phi \cdot \frac{A_{cloud}}{A_T}; \qquad \frac{\partial V}{\partial \Phi} = \frac{1}{A_T}\left[V \cdot A_{clear} - (V-G) \cdot A_{cloud}\right];$$

$$\frac{\partial V}{\partial A_{clear}} = -\frac{E}{A_T^2}(1-\Phi); \qquad \frac{\partial V}{\partial A_{cloud}} = -\frac{\Phi}{A_T}(V-G).$$

This definition of the error on total ozone was used in GDP 3.0, with s_E coming from the DOAS slant column fitting, s_Φ from the cloud pre-processing (in this case the ICFA fitting algorithm); s_G was set to zero and a fixed value of 1% was assumed for AMF errors. Improved error estimates are available for the total ozone algorithm, and we now discuss the error budget and the assignations used in the operational GDP 4.0 algorithm.

2.7.2 Error budget

In the pre-operational GDOAS algorithm developed off-line as part of the GODFIT project, typical errors on ozone slant columns, ozone AMFs, cloud fractions and ozone ghost columns were reported in [R2]. These error estimates are summarized below in Table 2; more details can be found in the appropriate sections in [R2].

Table 2. Estimation of error sources of the GDOAS total ozone retrievals (single pixel retrieval).

Error source	**Percent error**	
	SZA < 80°	**SZA > 80°**
Ozone slant column		
O_3 absorption cross-sections	<2	<2
Atmospheric (effective) temperature determination	<1.5	<3
Instrument signal-to-noise	0.5	<2
Instrument spectral stability (wavelength registration)	0.5	0.5
Solar I_0-effect	0.2	0.2
Ring and molecular Ring effect	<2	<2
Ozone Air Mass Factor		
Single wavelength calculation (325.5 nm)	<1	<2
O_3 profile	<1	<4
Surface albedo	0.3	0.3
Cloud fraction	0.8	0.8
Cloud top pressure	1	1
Ghost column	<2	<3
Tropospheric aerosols	0.2	0.2
Ozone vertical column (accuracy)		
Clear	<3.6	<6.4
Cloudy	<4.3	<7.2
Ozone vertical column (precision)		
Clear	<2.4	<4.9
Cloudy	<3.3	<5.9

The error budget has been separated into two parts: errors affecting the retrieval of slant columns (DOAS-related errors) and errors affecting the conversion of slant columns into vertical columns (AMF-related errors). We include the molecular Ring effect error under the DOAS heading. The DOAS-related (slant column) uncertainties quoted in Table 2 are, for the large part, extracted from the study performed as part of the GDP 3.0 Delta validation exercise [van Roozendael et al., 2002]. Errors due to the molecular Ring effect are derived from closed-loop retrieval tests presented in the GODFIT main validation report [R3].

Uncertainties related to cloud correction are estimated from error propagation of the uncertainties on the FRESCO cloud parameters. Errors relating to O_3 AMF values stem from sensitivity tests carried out using different settings for the AMF calculations (e.g. different O_3 profile climatologies). Several error sources are significantly enhanced at large solar zenith angles (typical of polar spring and autumn observations), and the error budget is given separately for low (<80°) and large (>80°) values of the SZA. Indeed, the uncertainty on the ozone AMF calculation is a strong function of the solar zenith angle (SZA), especially for SZA > 80°. Errors on AMFs will mostly depend on the shape of the ozone profile, as well as its column content. An upper limit of the AMF error (and its SZA dependence) can be obtained from consideration of the variability of O_3 AMFs calculated using a wide range of climatological ozone profiles. Figure 12 illustrates this variability for calculations based on the Fortuin and Kelder [1998] climatology.

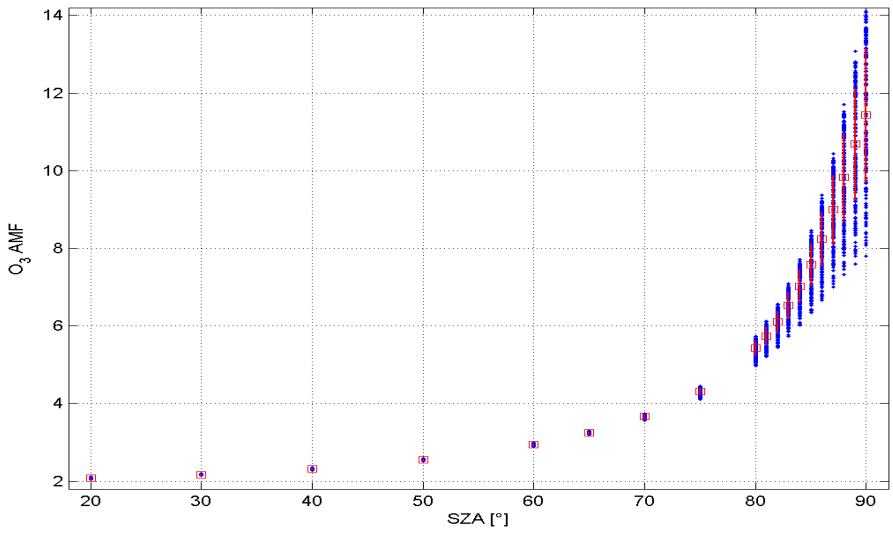

Figure 12. Ozone AMF variability based on the Fortuin/Kelder climatology.

2.7.3 GDP 4.0 total ozone error: operational baseline

We deal first with the slant column, cloud fraction and ghost column errors before defining the AMF error. We will adopt the following provisional choices:

s_E	as provided by the DOAS algorithm
s_Φ	as provided by the OCRA algorithm
s_G	30 %

The ghost column estimate here is a composite figure based on error contributions from a number of sources (in particular, the ROCINN estimate of cloud-top height error and the ozone profile uncertainty).

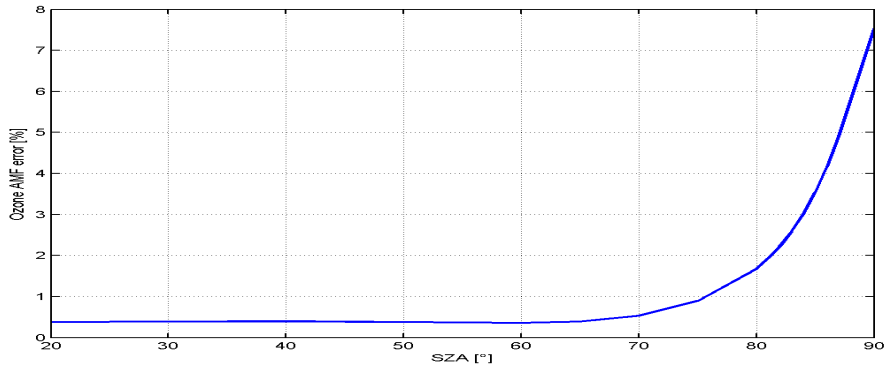

Figure 13. Ozone AMF percentage error as a function of SZA.

In GDP 4.0, the column-resolved TOMS v.8 climatology is used to adjust model O_3 profiles to actual conditions, and the error on O_3 AMFs is expected to be significantly lower than that shown in Figure 12. Nevertheless, higher uncertainties will still be present at large SZA. We will use the percentage error curve depicted in Figure 13; this is derived from the analysis presented in Figure 12 and scaled down by factor of 2 so that AMF uncertainties are consistent with provisional errors. Use of this curve will be reflected in larger uncertainty of the GDP 4.0 total ozone product for high SZA conditions.

3. THE OPERATIONAL ALGORITHM

3.1 The UPAS environment at DLR

UPAS (Universal Processor for UV/VIS Atmospheric Spectrometers) is a new-generation level 2 processing system for the generation of operational near real time and off-line trace gas retrieval products. UPAS takes as input the calibrated and geolocated Level 1 radiances from different sensors (e.g. GOME on ERS-2 and GOME-2 on METOP) and produces total columns of trace species such as O_3, NO_2 and BrO. UPAS is also capable of retrieving ozone profiles.

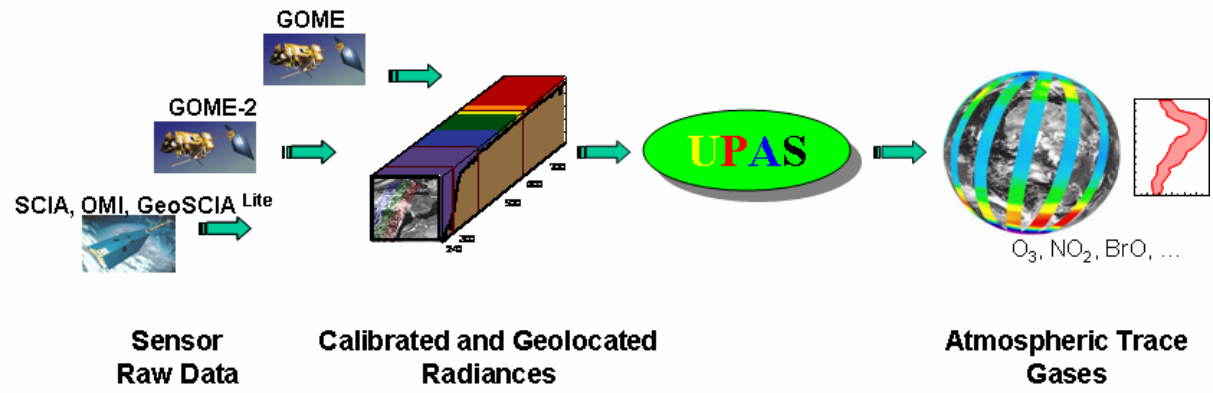

Figure 14. Overview of the UPAS system. UPAS can process calibrated and geolocated radiances from different spectrometers and produce total column of trace gases as well as ozone profiles.

The UPAS core is fully implemented in C++; the entire DOAS software is in C++ as are the AMF and LIDORT V2.2+ environments. The LIDORT model itself (written in FORTRAN 77) is called as a function. The GDP level 1-to-2 systems before GDP 4.0 used a mixture of FORTRAN and C code. At DLR, UPAS is now an operational system, and earlier versions of GDP have prototype status. With this UPAS/GDOAS upgrade, UPAS is now the new operational system for GOME total ozone and NO_2 processing, replacing the older GDP versions.

UPAS exploits the power of the object-oriented paradigm (inheritance and polymorphism) for the flexible definition and implementation of algorithm "families". This allows the system to switch easily between different algorithms for comparison purposes. Given this flexible structure, it is straightforward to integrate new retrieval algorithms into the system as and when they become available.

3.2 UPAS/GDOAS implementation: practicalities

3.2.1 Introduction

The initial algorithm for GDOAS was written at SAO in FORTRAN 77 on a Sun UNIX workstation, and was transferred to PCs at BIRA-IASB with Linux and Windows-based

operating systems in June 2003. The algorithm was then tested on whole orbits of GOME data, and linked to the validation software at BIRA. All GDOAS validation exercises reported under the ESA ITT in December [R2] and January [R3] were done on BIRA platforms.

The UPAS system already possessed a full DOAS fitting capability and a complete iterative AMF/VCD component based on LIDORT before the present GDOAS upgrade. (The LIDORT package is the only part of the code in F77). Hence, the implementation of these components involved changes to existing component units in C++, rather than the wholesale transferal of complete self-contained algorithms (in F77) from an external source. The molecular Ring correction is relatively straightforward, and this was reprogrammed in C++ for UPAS and verified off-line against the original source code.

Clearly, the new algorithm (UPAS/GDOAS at DLR) has been carefully verified against the external existing algorithm (GDOAS at BIRA) to ensure consistency. Verification issues for the DOAS and AMF/VCD components are discussed in the following two sections.

A number of other minor points can be discussed here. The OCRA/ROCINN cloud algorithms are implemented in UPAS/GDOAS at DLR only, while the ingestion of external FRESCO data is an option for both algorithms. Software to deliver Level 1 data in whole-orbit granules is the same. The major issue here is the conversion of geolocation information specified at fixed levels (at 70 km and at the spacecraft) in the Level 1b product to values at a user-specified atmospheric height in the Level 2 processing.

Exception handling is defined for the UPAS system, and will be fully compliant with previous DLR protocols in earlier GDP versions, and also with ESA software standards [A2]. We note here that LIDORT has its own error handling structure, which is incorporated in the larger whole. Experience with repeated calls to LIDORT has shown that the code is extremely robust, and LIDORT will never return errors in the normal run of things. Results on whole orbit data have indicated that the algorithm does indeed possess this robustness.

3.2.2 DOAS verification (O_3)

DOAS fitting in the original GDOAS algorithm was done with dedicated optical estimation inversion code [Rodgers, 2001] or with non-linear least squares fitting from the SLATEC library [Fong et al., 1993]. At BIRA, the DOAS fitting was then modified to match the WINDOAS fitting algorithm developed at BIRA for Windows-based PC retrieval of GOME data [Fayt and van Roozendael, 2001]. DOAS fitting in UPAS is a completely new implementation of the basic DOAS software in C++; it is based on a more up-to-date set of numerical libraries than those employed in the external GDOAS algorithm.

Given identical cross-sections and other reference spectra, it should be possible for the UPAS and external GDOAS codes to agree very closely. At the kick-off meeting for the GDP 4.0 upgrade in May 2004, it was reported that ozone slant columns for 4 test orbits were in agreement to better than 0.2%, a figure which is much lower than the overall accuracy that can be expected from this retrieval. Further testing has now reduced differences to below 0.02% for all solar zenith angles less than 85° (June 25, 2004), and better than 0.08% in all cases.

The efficacy of the "Post level 1" additional solar spectrum shift derived by cross-correlation in the 325-335 nm window was also checked for 6 GOME orbits in the 1998-2000 period. The stability of the improved scheme was tested by fitting of ozone cross-section shifts (instead of using the fixed pre-shift); in this way the optimum pre-shift value of +0.016 nm was seen to give stable results for all orbits.

3.2.3 AMF/VCD verification (O_3)

As with the DOAS component, UPAS has a fully functional AMF/VCD iteration scheme, and the major implementation issue is to ensure that this component performs consistently in its external GDOAS and operational UPAS/GDP 4.0 manifestations. The UPAS scheme is able to perform simulations "on-the-fly" with calls as needed to the LIDORT F77 code. To achieve consistency, it was necessary to modify the UPAS code to use the pressure levels found in the TOMS V8 climatology. In this way the codes can process the same atmospheric set-up data, and in June 2004 it was reported that the two codes were able to generate exactly the same optical property inputs for their calls to LIDORT. Surface topography and albedo databases were also checked for consistency, as was the molecular Ring correction implementation.

LIDORT sphericity issues

The LIDORT Version 2.2+ model [Spurr, 2003] was installed in UPAS in October 2003 to deal with wide-angle off-nadir geometry. [This work was done for GOME-2 algorithm development as part of a EUMETSAT visiting scientist grant; GOME-2 has a 1920 km swath]. In addition to the pseudo-spherical treatment of solar beam attenuation, LIDORT 2.2+ has several sphericity corrections to deal with curved shell geometry along the line-of-sight (LOS). LIDORT 2.2+ makes calls to the LIDORT V2.3 code, which has *exactly* the same capability (as far as simulating radiances) as that for the LIDORT V2.5 package that was developed for the GODFIT project. V2.3 and V2.5 are pseudo-spherical codes. Thus it should be possible *mutatis mutandis* to reproduce radiances precisely, at least for an ordinary pseudo-spherical computation.

An important sphericity issue arises with GOME polar view retrievals; these will also be part of the GOME data record reprocessing. In this viewing mode, scan angles are between 40 and 50 degrees – this is far enough from the nadir to require the use of an LOS sphericity correction in the LIDORT calls. For complete consistency, one should really use the same sphericity enhancements for *all* AMF simulations in order to maintain consistency between polar mode and nominal scan mode results. With the LIDORT V2.2+ implementation, GDP 4.0 has the ability to simulate radiances more accurately for GOME polar mode viewing.

Geometrical weighting

Another simulation issue concerns the back-scan GOME pixels. With the 3 forward scans, a single choice of geolocation viewing geometry (at the mid-scan point) is sufficiently accurate for radiance (and hence AMF) simulations. However, the scan-angle range is much greater for the back scan (-31º to +31º), and one needs to do more RT calculations to properly account for varying LOS zenith angle. The solution adopted for GDP versions up to 3.0 has been to use all three backscan geometries (start, mid-point and end of scan) to make three

separate radiance simulations, which are then combined in the ratios 1:4:1. This weighting is essentially a parabolic integration of the spot radiance over the scan angle, with the largest proportion (2/3) from a calculation at the center-scan geometry.

The issue of scan-angle integration of radiance has been looked more systematically at KNMI in the context of GOME ozone profile retrieval. Radiances should be integrated (over time) over the readout duration and one complication here is that the scan mirror does not move uniformly with time during the back-scan. It was found that an approximation of the scan-angle integration by means of 2-point Gauss-Legendre quadrature gives good accuracy for radiance simulations [R. van Oss, private communication]. Pairs of scan-angle abscissa can be determined readily for all types of (non polar view) scan modes.

Further off-line simulations have shown that a 3-point quadrature gives sufficient accuracy for the back scans. This will now be the GDP 4.0 default for the back scans. The current default for GDP 4.0 forward scans will be to use 2-point quadrature. Quadrature angles are calculated on the fly using variation of the line-of-sight angles. Angles are linearly corrected using pre-computed coefficients due to changing scan mirror speed for the back-scan pixels. In all cases there is enough performance margin to cover these options.

AMF verification

External GDOAS uses LIDORT only in the pseudo-spherical approximation with a single TOA input geometry. For the verifications with UPAS, the LIDORT V2.2+ settings coincided with those for the external GDOAS. In June 2004, it was reported that with LIDORT control and optical property inputs checked, AMF results for forward-scan clear sky scenarios were in excellent agreement for forward scan pixels (agreements better than 0.4%, well within the target). The main source of any remaining differences is due to slightly different input geometries created by two different geolocation conversion methods (UPAS uses the more accurate ERS-2 orbit propagator, external GDOAS has a simple conversion module).

VCD verification

External GDOAS results were compared with UPAS/GDP 4.0 total column results for the verification, and also with GDP 3.0 results for a number of orbits. All these results were compared to a subset of the ground-based stations in a "pre-validation" exercise (reported at the August 5th 2004 progress meeting). It was clear that UPAS/GDP 4.0 results (with both FRESCO and OCRA/ROCINN cloud information) and external GDOAS results (FRESCO clouds) behave similarly and show similar validation margins; both sets are (as expected) are in better agreement with ground data than the GDP 3.0 results.

Some problems were noted with the use of FRESCO data. The data is not available for backscan pixels, it is often absent at the start and end of an orbit, and the VCD testing was not done for pixels without suitable FRESCO data. It was noted that the results with FRESCO in UPAS would be subject to some changes owing to a recent revision of the FRESCO algorithm – a new LUT for UPAS was prepared for the validation phase.

The verification phase yielded excellent agreements for matching slant columns and AMFs based on identical setups. It became clear that the UPAS GDOAS implementation offered additional benefits. Already noted is the more accurate ERS propagator software, the use of

spherical corrections in LIDORT, better interpolation schemes and more up-to-date reference data, plus the use of area-weighting (tessellation) for surface property assignations. In summary, differences between the operational UPAS/GDP 4.0 baseline and the off-line GDOAS algorithm implementation may be listed below:

1. Use of OCRA/ROCINN to retrieve cloud parameters
2. Use of additional sphericity corrections in the UPAS LIDORT V2.2+ calculations
3. Use of the ERS propagator to deliver viewing geometry inputs from ephemeris data
4. Latitude interpolation of the TOMS Version 8 ozone profile climatology
5. Newer topography database (GTOPO30)
6. Combined use of GOME LER and TOMS (380 nm) surface reflectivity data
7. Use of area-weighting tessellation to deliver surface albedo and ground topography

3.2.4 NO_2 verification

The *external* GDOAS algorithm was applied only to total ozone, and a direct verification of the GDP 4.0 NO_2 application is therefore not possible. Nevertheless, the considerable overlap between the two systems allows for a partial verification. Slant column and AMF/VCD results were also compared with GDP 3.0 output for a small number of orbits in order to check consistency.

The DOAS part of the NO_2 GDOAS algorithm was verified in the same manner as done for the O_3 fitting: output from the WINDOAS slant column fitting code was compared directly with that from UPAS/GDOAS. Results are better than 1% (in most cases better than 0.5%). Comparisons with GDP 3.0 for a section of 5 orbits show reduced RMS with the new fitting algorithm, and reduced slant columns (up to 10-15% at low latitudes) in the GDP 4.0; differences with GDP 3.0 are within reported fitting precisions.

Before the upgrade to GDP 4.0, the NO_2 AMF implementation was based on single scatter RT calculations and multiple scatter look-up corrections, based on a single NO_2 profile. The composite climatology of stratospheric NO_2 profiles from Lambert and Granville [2004] selected for the GDP 4.0 baseline was incorporated in the external GDOAS software, and an "atmosphere set-up" for the NO_2 AMF established for the total ozone UV window. This climatology and set-up was installed in UPAS, and the set-up checked to ensure that NO_2 profiles were delivered on the baseline pressure grid for the new algorithm. The UPAS LIDORT configuration was then used to compute NO_2 AMFs in the visible at 437.5 nm, and the results were consistent with expectations.

Comparisons with GDP 3.0 AMF values show agreements generally within 2% except at high latitudes; this is to be expected given different input profile choices and different radiative transfer implementations. GDP 4.0 results are also consistent with NO_2 AMF values calculated recently using the DAK model at KNMI [Boersma and Eskes, private communication]. Comparisons of NO_2 VCD values between GDP 3.0 and GDP 4.0 are also consistent; GDP 4.0 results are slightly smaller, with differences at low latitudes mainly due to slant column differences.

3.2.5 OCRA/ROCINN verification

These algorithms were verified by comparison with ATSR-2 data provided by RAL. Cloud parameters (cloud fraction and cloud-top height) are determined from ATSR-2 data using infrared brightness temperature algorithms and the instrument's stereo viewing capability. ATSR-2 measures simultaneously with GOME on ERS-2, but it has a smaller field of view (pixel resolution ~1.1 km), so GOME narrow-swath orbits were selected. Measurement data for one year (April 1998 to March 1999) were used in the verification (331 orbits). FRESCO results were also verified for this yearlong data set.

ATSR-2 comparisons show that OCRA/ROCINN gives better results on average than those from FRESCO. Differences in fraction and cloud-top height are smaller, and standard deviations of these differences are lower. Cloud-top heights from the ROCINN algorithm also show reduced scatter against ATSR-2 values. Also checked in this verification was the effect of various cloud algorithms on the total ozone. GDP 3.0 total ozone results (made using the ICFA/ISCCP cloud pre-processing algorithm) were plotted alongside UPAS/GDP 4.0 results (FRESCO and OCRA/ROCINN cloud algorithms) and compared to ground total ozone. The spread shows a clear improvement from GDP 3.0 to 4.0.

3.2.6 Performance issues

From the performance viewpoint, the major new feature in GDP 4.0 is the computation of AMFs using explicit calls to an RT model - the first time this has been attempted for *operational* total column retrieval from GOME. It is expected that the algorithm will be slower than GDP 3.0, which has a fast neural-network parameterization for AMFs. However, the processing time for one orbit is still well within the data turnover rate (see below).

Doing RTM simulations from scratch is the time-consuming step, and this depends on the two discretizations used in LIDORT – the number of vertical layers and the number of discrete ordinate streams. For a 13-layer atmosphere with 8 discrete ordinates in total (this is the baseline), a single LIDORT call will return the backscatter radiance in a small fraction of a second.

Based on these considerations, we make the following estimates. Assuming an orbit with 2000 footprints, 90% of which are partially cloudy (requiring dual cloud/clear sky computations), an average of 3.5 iterations for the AMF/VCD scheme, and geometrical weighting for the back-scans (2 geometries), we find that there are approximately 60,000 model calls to LIDORT during the processing of an orbit granule. On the fastest PC available at BIRA (a Dell with 2.8 GHz processor), it takes around 4 minutes to complete processing for one orbit, once the Level 1 data has been extracted. The processing time for the whole algorithm is about twice this period – the other main time-consuming task is the ingestion of one granule of Level 1b data. Thus it is clear that there is ample capacity for real-time data turnover.

For the operational processing we have the following performance estimation. The UPAS system is based on client-server architecture, and this makes it possible to run the system with an unlimited number of processing nodes. The GDP 4.0 operational reprocessing system is based on 10 Linux PCs, each with 2 processors (3 GHz Intel CPUs). The UPAS system and

its constituent retrieval algorithms have been optimized for processing performance. The complete processing of one GOME orbit takes around 3 minutes on a single CPU, and on this basis, the reprocessing of the complete GOME data set can be done in just a few days.

4. SENSITIVITY AND VALIDATION

4.1 Sensitivity issues for GDP 4.0

With a tight schedule to complete the reprocessing of the GOME total ozone record by the end of 2004, there has been limited opportunity for sensitivity studies following the implementation and verification of GDP 4.0 in summer 2004; this phase was succeeded immediately with the validation itself. We discuss below some sensitivity tests carried out in response to questions raised by ESA during the delta validation for the three consortium algorithms (GDOAS, TOGOMI, GOTOCORD) sponsored under the ESA ITT aegis. This work was reported in the GDOAS Delta Validation report [R3] presented in final form in January 28th, 2004.

4.1.1 Choice of temperature

In the two-step DOAS approach used here, the largest impact of atmospheric temperature is through the temperature-dependence of the ozone absorption cross-sections. This dependence is accounted for in the DOAS algorithm by fitting two ozone spectra at two different temperatures. The accuracy of this approach (see [Lambert et al., 2002] for validation results) is limited towards (1) large SZA due to the breakdown of the optically thin approximation, (2) extreme stratospheric temperatures (due to non-linearity in the temperature dependence of the ozone cross-sections), and (3) by the intrinsic accuracy of the laboratory cross-sections.

It is possible that instrument degradation also has an impact on the accuracy of the effective temperature determination. This has not been tested explicitly, but results from GDOAS overpass processing over Hohenpeissenberg and Lauder, extending from 1996 until 2003 and retrieved with no particular effort to compensate for known GOME degradation problems, suggest that the DOAS algorithm is stable and not strongly influenced by the degradation of the instrument (see Figures 4 and 5 in [R3]).

4.1.2 Choice of fitting window

For the GODFIT project, a number of direct fitting studies were carried out for a smaller window shifted a little towards the visible (331-336 nm). There are advantages to be gained from this choice (lower temperature sensitivity, and ozone slant column retrievals should be more accurate at large solar zenith angles because of reduced ozone optical depth. On the other hand, we expect larger noise at small solar zenith angles in tropical regions; this might be an issue for accurate long-term trend monitoring. For this reason in particular, it was decided to remain with the standard GDP choice (325-335 nm) for the GDOAS studies reported in [R3]; an added advantage is that validation against GDP 3.0 is clear.

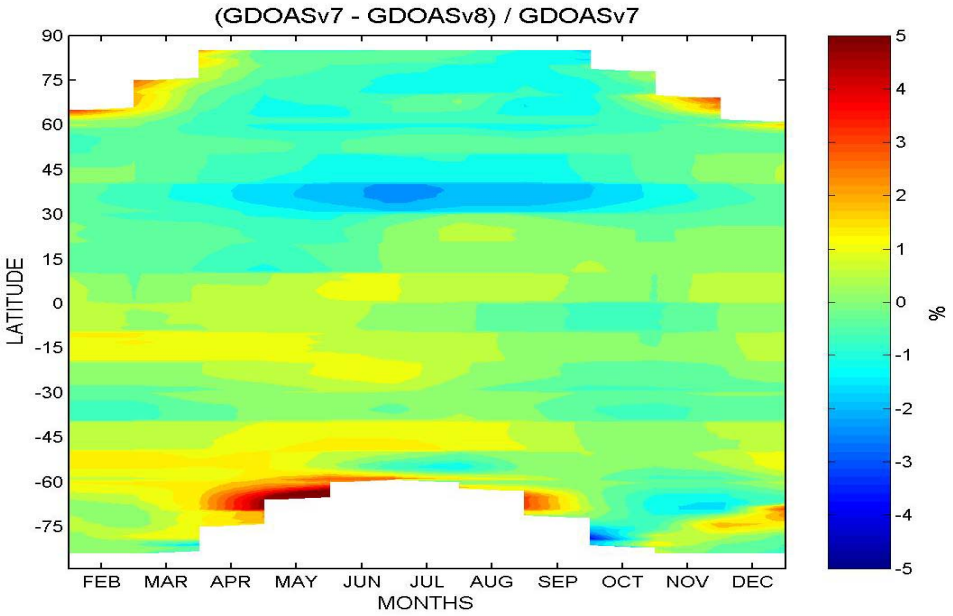

Figure 15. Relative differences in GDOAS GOME total ozone retrieved using the two TOMS version 7 and version 8 ozone profile climatologies. Differences are mostly significant in Polar Regions, close to the terminator, as well as in Northern tropical regions around the place of minimum GOME solar zenith angle.

4.1.3 Impact of ozone profile choice

Since the iterative AMF/VCD algorithm relies on an ensemble of ozone profiles to define the profile-column map needed to the iteration, the choice of ozone profile climatology is important. Ozone profile shape is a key factor controlling the accuracy of the total ozone retrieval, especially in regions of high-latitudes where the ozone profile-shape sensitivity of the AMFs is enhanced by the extreme variations in the ozone field (e.g. ozone hole) combined with large solar zenith angles.

The GDOAS code has been tested using both TOMS version 7 and version 8 ozone profiles climatologies. The two climatologies were outlined in Section 2.3.2, and the GDP 4.0 baseline is TOMS version 8, which is resolved in total column, latitude and season.

Differences in retrieved total ozone columns using the two climatologies are shown in Figure 15. The largest differences are found in Polar Regions (especially in the Southern hemisphere) close to the terminator where GOME solar zenith angles are at their maximum. A surprisingly large sensitivity is also found in the Northern sub-tropics during summer when the GOME SZA is at minimum.

4.1.4 Stratospheric aerosol

Stratospheric aerosols, if emitted in large quantities as ejected material from a major volcanic eruption (Mt. Pinatubo in 1991 is a good example), will be a source of significant error in the GOME total ozone retrieval. Scattering properties of the atmosphere will be strongly altered

at stratospheric altitudes. Due to the lack of time and the focus on GDOAS validation, this issue has not yet been examined. We believe that this aspect is important and deserves further study to quantify the impact of volcanic aerosols and eventually devise a strategy to account for it in operational total ozone retrieval.

4.2 Introduction to the GDP 4.0 validation

4.2.1 Methodology and validation tools

The validation of currently operational GOME data products, on the near-global scale as well as in the long term, has been coordinated at BIRA-IASB using ground-based observations from the Network for the Detection of Stratospheric Change (NDSC). NDSC instruments (UV-visible and FTIR spectrometers, lidars, microwave radiometers, Dobson and Brewer spectrophotometers, and ozonesondes) are carefully maintained and well documented. Most of these instruments contribute to WMO's Global Atmospheric Watch (GAW) program through participation in the NDSC and the World Ozone and Ultraviolet Data Center (WOUDC). The GOME validation database started before the GOME launch in 1995, and has been extended regularly to include newly acquired data.

The GDP 4.0 Validation Report [R12] uses the GDOAS delta validation document [R3] as a starting point; the validation methodology is the same. There are many more ground stations included in the GDP 4.0 validation and a much greater selection of orbits (4910 as opposed to 2257). The GDP 4.0 validation also contains a much more extensive inter-comparison with TOMS Version 8 results than was possible earlier this year in the pre-validation GDOAS phase. All GOME pixel types (up to SZA 88º) were considered in the comparison with TOMS v.8 ozone data. Relative agreements between GDP 4.0 and ground-based total ozone values were contrasted to similar results from ground-based inter-comparisons applied to both the GDP 3.0 and TOMS v.8 ozone products.

For comparison studies associated with validation, one must deal with a variety of problems arising from the remote sensing nature of the ozone measurement to be validated and the geophysical nature of the observed ozone field. These include differences in spatial and temporal resolution, differences in weighting functions, differences in measurement time (mid-morning GOME against twilight ground-based UV-visible spectrometers), natural variability, inhomogeneity of atmospheric parameters along the line-of-sight, etc.

For the dependency analyses, we characterize cyclic signatures in GOME versus ground-based ozone comparisons by fitting time-series of individual comparison data points to simple cosine functions via:

$$R = A + B \cdot \cos\left(2\pi\left[t - \Phi\right]\right). \tag{23}$$

Here:

- R = relative difference (%) between GDP and correlative O_3 measurements
- A = offset parameter, representing the mean total ozone relative difference
- B = amplitude of the annual wave variation
- t = time in decimal year
- Φ = phase of the cosine function

In the GDP 4.0 validation, time series analyses were applied equally to GDP 3.0 and TOMS data, as well as to the GDP 4.0 results themselves.

4.2.2 GDP 4.0 validation digest

The GDP 4.0 algorithm has three main improvements over that for GDP 3.0: (a) an improved correction for ozone absorption distortion due to inelastic rotational Raman scattering by air molecules; (b) a new cloud treatment for the retrieval of three auxiliary pieces cloud information, a (c) further improvements to the AMF calculation using on-the-fly radiative transfer modeling. Validation of the GDP 4.0 algorithm showed a marked improvement in retrieved total ozone values in two important aspects.

First and most significant, there was a drastic reduction of nearly all remaining cyclic signature dependencies on latitude, season, SZA and ozone column in the GOME versus ground-based total ozone comparisons; this was identified as an outstanding issue for GDP 3.0. Annual wave amplitudes were reduced by a factor of two on average, with the best improvement at northern high latitudes. In contrast, no obvious improvement was found over Antarctic stations. Likewise, solar zenith angle and total ozone column dependencies reported in GDP 3.0 were very substantially reduced in GDP 4.0. The latter improvement is mostly attributed to the use the new molecular Ring correction that accounts properly for the impact of ozone absorption line filling. Possible reasons (which need to be determined) for the remaining discrepancies observed at Southern high latitudes are: (1) systematic errors in the GDP 4.0 algorithm specific to Antarctic regions; (2) co-location problems between satellite and ground-based data that may introduce bias in the comparisons because of strong gradients in the O_3 field; and (3) systematic errors in ground-based data (difficulties maintaining accuracy of total ozone spectrometers in remote Southern polar regions).

Secondly, validation results showed that GDP 4.0 total ozone retrievals were on average 1.5% larger than those from GDP 3.0; this is in much better overall agreement with ground-based measurements. In general, the average agreement of GDP 4.0 with correlative ozone column measurements is now at the “percent level”, that is, within the precision level of ground-based sensors when the latter are corrected for their own dependencies on the season, solar elevation, temperature etc. At polar latitudes, and at solar zenith angles larger than 80°, the agreement is slightly worse; however, average differences at low solar elevation usually do not exceed 5%. A remarkable feature of the reprocessed GOME GDP 4.0 total ozone data record is that, despite the anticipated degradation of the instrument with time, the total column products do not suffer from any long-term drift of quality. This is the case even in late 2004, when the degradation of the UV ozone channel has reached 42.9%. Further, GOME gives a consistent picture of the global ozone field with temporal signals and spatial structures similar to those observed by other high-quality sensors; this is borne out with the good overall agreement between GDP 4.0 and TOMS V.8 results.

The GOME GDP 4.0 total NO_2 product has also been validated from pole to pole, with comparisons to ground-based measurements of the NDSC network of SAOZ/DOAS UV-visible spectrometers and Fourier Transform Infrared spectrometers, and to global data from the HALOE and POAM satellite sensors and tropospheric and stratospheric modeling tools. GDP total NO_2 is in reasonable agreement with ground-based and other satellite

measurements: within ±5 10^{14} molec.cm^{-2} in areas of low tropospheric NO_2 and within ±8 10^{14} molec.cm^{-2} in areas of very low slant column of NO_2. Although it is difficult to make a precise evaluation of the NO_2 total column accuracy (due to various problems such as the photochemical diurnal cycle of NO_2), the overall accuracy is estimated to fall within the 5% to 10% range, provided that the contribution of tropospheric NO_2 to the vertical column remains low. GDP total NO_2 has larger errors under certain circumstances, e.g., in the South Atlantic Anomaly and over polluted areas. In the latter case, current NO_2 AMF values and effective absorption temperatures calculated for pure stratospheric scenarios do not account for variations in the tropospheric burden of NO_2 and are consequently subject to systematic errors. For scenarios of extreme pollution, modeling results suggest that AMF errors can lead to an underestimation of the actual NO_2 vertical column amount by a factor of two.

ACKNOWLEDGEMENTS

Special thanks are due to Yakov Livschitz (DLR) for handling the UPAS/GDOAS GDP 4.0 implementation and verification. We thank also DLR colleagues Thomas Ruppert and Pieter Valks for their contributions. Werner Thomas (now at DWD) was a part of the DLR team in 2003 supporting GDOAS work. At BIRA-IASB, thanks are due to Jean-Christopher Lambert for many contributions and to Caroline Fayt for software support. At AUTH, thanks to Dimitris Balis for the GDP 4.0 validation work. At S&T, thanks to Pepijn Kenter for software testing support. At DLR, we thank Bernd Aberle for help with quality assurance for the reprocessed data, and Leonid Butenko for help with HDFS format conversion.

Many scientists at a number of institutions in Europe and America have made contributions to the GOME data processing effort. In particular, we would like to thank colleagues from Uni. Bremen (Germany), KNMI (Netherlands), Uni. Heidelberg (Germany), BIRA-IASB (Belgium), DLR (Germany), SAO (USA), SRON (Netherlands), NASA Goddard (USA), RAL (Great Britain) and AUTH (Greece). We would also like to thank colleagues from the agencies: ESA-ESTEC (Netherlands), ESA-ESRIN (Italy) and EUMETSAT (Germany).

We would like also to thank Claus Zehner (ESA-ESRIN) for his steadfast support of GDP and the GDOAS enterprise.

5. REFERENCES

Aliwell, S. R., M. van Roozendael, P. V. Johnston, A. Richter, T. Wagner, D. W. Arlander, J. P. Burrows, D. J. Fish, R. L. Jones, K. K. Tørnkvist, J.-C. Lambert, K. Pfeilsticker, and I. Pundt, Analysis for BrO in zenith-sky spectra: An intercomparison exercise for analysis improvement, *J. Geophys. Res.,* **107**, D14, doi: 10.1029/2001JD000329, 2002.

Bass, A.M., and R.J. Paur, The Ultraviolet Cross Sections of Ozone: I. The Measurements, in Atmospheric Ozone, Proceedings of the Quadrennial Ozone Symposium, edited by C. S. Zerefos and A. Ghazi, D. Reidel Publishing Company, Halkidike, 1984.

Berk, A., L. S. Bernstein, and D.C. Robertson, MODTRAN: A moderate resolution model for LOWTRAN-7, GL-TR-89-0122, *Geophysics Laboratory*, Hanscomb AFB, MA 07132, 1989.

Bhartia, P. K., Algorithm Theoretical Baseline Document, TOMS v.8 Total ozone algorithm, 2003 (http://toms.gsfc.nasa.gov/version8/version8_update.html)

Boersma, K. F., H. J. Eskes, and E. J. Brinksma, Error analysis for tropospheric NO_2 retrieval from space, *J. Geophys. Res.*, **109**, D04311, doi:10.1029/2003JD003962, 2004.

Bowker, D. E., R. E. Davies, D. L. Myrick, K. Stacy, and W. T. Jones, Spectral Reflectances of Natural Targets for Use in Remote Sensing Studies, NASA Reference Publication, 1139, 1985.

Bodhaine, B., N. Wood, E. Dutton, and J. Slusser, On Rayleigh optical depth calculations, *J. Atmos. Ocean. Tech.*, **16**, 1854-1861, 1999.

Burrows, J. P., A. Dehn, B. Deters, S. Himmelmann, A. Richter, S. Voigt, and J. Orphal, Atmospheric Remote-Sensing Reference Data from GOME: Part 1. Temperature-dependent absorption cross-sections of NO_2 in the 231-794 nm range, *J. Quant. Spectrosc. Radiat. Trans.*, **60**, 1025-1031, 1998.

Burrows, J. P., A. Richter, A. Dehn. B. Deters, S. Himmelmann, S. Voigt and J. Orphal, Atmospheric remote sensing reference data from GOME: Part 2. Temperature-dependent absorption cross-sections of O_3 in the 231-794 nm range, *J. Quant. Spectrosc. Radiat. Transfer*, **61**, 509-517, 1999a.

Burrows, J. P., M. Weber, M. Buchwitz, V. V. Rozanov, A. Ladstaetter-Weissenmeyer, A. Richter, R. de Beek, R. Hoogen, K. Bramstadt, K.-U. Eichmann, M. Eisinger, and D. Perner, The Global Ozone Monitoring Experiment (GOME): mission concept and first scientific results, *J. Atmos. Sci*, **56**, 151-175. 1999b.

Chance, K., Analysis of BrO measurements from the Global Ozone Monitoring Experiment, *Geophys. Res. Lett.*, **25**, 3335-3338, 1998.

Chance, K., and R. J. D. Spurr, Ring effect studies: Rayleigh scattering including molecular parameters for rotational Raman scattering, and the Fraunhofer spectrum, *Applied Optics*, **36**, 5224-5230, 1997.

Fayt, C., and M. van Roozendael, WINDOAS Users Manual, http://www.oma.be/BIRA-IASB/Molecules/BrO, BIRA-IASB, Brussels, 2001.

Fong, K. W., et al., Guide to the SLATEC common mathematical library, http://www.netlib.org/slatec/guide, 1993.

Fortuin, J. P. F., and H. Kelder, An ozone climatology based on ozonesonde and satellite measurements, J. Geophys. Res., **103**, 31709-31734, 1998.

Grainger, J. F., and J. Ring, Anomalous Fraunhofer Line Profiles, *Nature*, **193**, 762, 1962.

Greenblatt, G. D., J. J. Orlando, J. B. Burkholder, and A. R. Ravishankara, Absorption measurements of oxygen between 330 and 1140 nm, *J. Geophys. Res.*, **95**, 18577-18582, 1990.

Herman, J. R, and E. A. Celarier, Earth surface reflectivity climatology at 340 nm to 380 nm from TOMS data, *J. Geophys. Res.*, **102**, 28003-28011, 1997.

Kneizys, F. X., E. P. Shettle, L. W. Abreu, J. H. Chetwynd, G. P. Anderson, W. O. Gallery, J. E. A. Selby, and S. A. Clough, Users Guide to LOWTRAN 7, Air Force Geophysics Laboratory, Environmental Research Papers, No. 1010, AFGL-TR-88-0177, 1988.

Koelemeijer, R. B. A., J. F. de Haan, and P. Stammes, A database of spectral surface reflectivity in the range 335--772 nm derived from 5.5 years of GOME observations, *J. Geophys. Res.*, **108**, 4070, doi:10.1029/2002JD0024, 2003.

Koelemeijer, R. B. A., and P. Stammes, A fast method for retrieval of cloud parameters using oxygen *A* band measurements from the Global Ozone Monitoring Experiment, *J. Geophys. Res.*, **106**, 3475-3490, 2001.

Kuze, A., and K. V. Chance, Analysis of Cloud-Top Height and Cloud Coverage from Satellites Using the O_2 *A* and *B* Bands, *J. Geophys. Res.*, **99**, 14481-14491, 1994.

Lambert, J.-C., M. van Roozendael, M. De Maziere, P. C. Simon, J.-P. Pommereau, F. Goutail, A. Sarkissian, and J. F. Gleason, Investigation of pole-to-pole performances of spaceborne atmospheric chemistry sensors with the NDSC, *J. Atmos. Sci.*, **56**, 176-193, 1999.

Lambert, J.-C., M. van Roozendael, P. C. Simon, J.-P. Pommereau, F. Goutail, J. F. Gleason, S. B. Andersen, D. W. Arlander, N. A. Bui Van, H. Claude, J. de La Noe, M. de Maziere, V. Dorokhov, P. Eriksen, A. Green, K. K. Tornkvist, B. A. Kastad Hoiskar, E. Kyrø, J. Leveau, M.-F. Merienne, G. Milinevsky, H. K. Roscoe, A. Sarkissian, J. D. Shanklin, J. Stähelin, C. Wahlstrom-Tellefsen, and G. Vaughan, Combined characterization of GOME and TOMS total ozone measurements from space using ground-based observations from the NDSC, *Adv. Space. Res.*, **26**, 1931-1940, 2000.

Lambert, J.-C., et al., ERS-2 GOME GDP 3.0 Implementation and Delta Validation Report for GOME Level-1-to-2 Data Processor Upgrade to Version 3.0, ERSE-DTEX-EOAD-TN-02-0006, 2002.

Lambert, J.-C., and J. Granville, Harmonic climatology of stratospheric NO2, BIRA-IASB, Brussels, 2004.

Leue, C., M. Wenig, T. Wagner, O. Klimm, U. Platt, and B. Jaehne, Quantitative analysis of NO_2 emissions from Global Ozone Monitoring Experiment satellite image sequences, *J. Geophys. Res.*, **106**, 5493-5505, 2001.

Loyola, D., B. Aberle, W. Balzer, K. Kretschel, E. Mikusch, H. Muehle, T. Ruppert, C. Schmid, S. Slijkhuis, R. Spurr, W. Thomas, T. Wieland, and M. Wolfmueller, Ground Segment for ERS-2 GOME Data Processor, 3rd Symposium on Space in the Service of our Environment, Florence, Italy, *ESA SP-414*, 591-597, 1997.

Loyola, D., M. Bittner, B. Aberle, W. Balzer, C. Bilinski, S. W. Dech, R. E. Meisner, W. Mett, and T. Ruppert, GOME near-real-time service, *ESA Earth Observation Quarterly*, **58**, 41-43, 1998.

Loyola, D., and T. Ruppert, A new PMD cloud-recognition algorithm for GOME, *ESA Earth Observation Quarterly*, **58**, 45-47, 1998b.

Loyola, D., Parameterization of AMFs using artificial neural networks, ESAMS'99 - European Symposium on Atmospheric Measurements from Space, 709-713, *ESA WPP-161*, Noordwijk, The Netherlands, 1999.

Loyola, D., Cloud Retrieval for SCIAMACHY, *ERS-ENVISAT Symposium*, Gothenburg, 2000.

Loyola, D., Automatic Cloud Analysis from Polar-Orbiting Satellites using Neural Network and Data Fusion Techniques, *IEEE International Geoscience and Remote Sensing Symposium*, Alaska, **4**, 2530-2534, 2004.

Martin, R., K. Chance, D. Jacob, T. Kurosu, R. Spurr, E. Bucsela, J. Gleason, P. Palmer, I. Bey, A. Fiore, Q. Li, R. Yantosca, and R. Koelemeijer., et al., An improved retrieval of tropospheric nitrogen dioxide from GOME, *J. Geophys. Res., 107*, 4437, 2002.

Matthews, E., Global Vegetation and Land Use: New High-Resolution Data Bases for Climate Studies, *J. Clim. Appl. Met.*, **22**, 474-487, 1983.

Palmer, P. I., D. J. Jacob, K. V. Chance, R. V. Martin, R. J. D. Spurr, T. P. Kurosu, I. Bey, R. Yantosca, A. Fiore, and Q. Li, Air-mass factor formulation for spectroscopic measurements from satellites: Application to formaldehyde retrievals from the Global Ozone Monitoring Experiment, *J. Geophys. Res.*, **106**, 14539-14556, 2001.

Paur, R. J., and A.M. Bass, The Ultraviolet Cross Sections of Ozone: II. Results and Temperature Dependence, in Atmospheric Ozone, Proceedings of the Quadrennial Ozone Symposium, edited by C. S. Zerefos and A. Ghazi, D. Reidel Publishing Company, Halkidike, 1984.

Platt, U., Differential optical absorption spectroscopy (DOAS), in Air monitoring by spectroscopic techniques, ed. M. Sigrist, *Chem. Anal. Ser.*, **127**, 27-84, 1994.

Richter, A., and J. P. Burrows, Tropospheric NO_2 from GOME measurements, *Adv. Space Res.*, **29**, 1673-1683, 2002.

Rodgers, D. C, Inverse Methods for Atmospheres: Theory and Practice, *World Scientific Press*, 2001.

Rothman, L., et al., The HITRAN molecular spectroscopic database: edition of 2000 including updates through 2001, , *J. Quant. Spectrosc. Rad. Transfer*, **82**, 5-44, 2003.

Rozanov, V. V., D. Diebel, R. J. D. Spurr, and J. P. Burrows, GOMETRAN : Radiative Transfer Model for the Satellite Project GOME, the Plane-Parallel Version, *J. Geophys. Res.*, **102**, 16683-16695, 1997.

Sarkissian, A., H. K. Roscoe, D. Fish, M. van Roozendael, M. Gil, H. B. Chen, P. Wang, J.-P. Pommereau, and J. Lenoble, Ozone and NO_2 air-mass factors for zenith-sky spectrometers: Intercomparison of calculations with different radiative transfer models, *Geophys. Res. Lett.*, **22**, 1113-1116, 1995.

Schiffer, R. A., and W. B. Rossow, The international satellite cloud climatology project ISCCP: The first project of the world climate research program, *Bull. Am. Meteorol. Soc.*, **54**, 779-784, 1983.

Siewert, C., A concise and accurate solution to Chandrasekhar's basic problem in radiative transfer, *J. Quant. Spectrosc. Radiat. Transfer*, **64**, 109-130, 2000.

Slijkhuis, S., A. von Bargen, W. Thomas, and K. Chance, Calculation of Under-sampling correction spectra for DOAS spectral fitting, ESAMS'99 - European Symposium on Atmospheric Measurements from Space, Noordwijk, The Netherlands, *ESA WPP-161*, 563-569, 1999.

Slijkhuis, S., CHEOPS-GOME: Study on seasonal effects on the ERS-2/GOME Diffuser BSDF, *CH-TN-DLR-GO-0001*, Issue 1, 2004.

Spurr, R. J. D., Improved climatologies and new air mass factor look-up tables for O_3 and NO_2 column retrievals from GOME and SCIAMACHY backscatter measurements, ESAMS'99 - European Symposium on Atmospheric Measurements from Space, Noordwijk, The Netherlands, *ESA WPP-161*, 277-284, 1999.

Spurr, R. J. D., T. P. Kurosu, and K. V. Chance, A Linearized discrete Ordinate Radiative Transfer Model for Atmospheric Remote Sensing Retrieval, *J. Quant. Spectrosc. Radiat. Transfer*, **68**, 689-735, 2001.

Spurr, R. J. D., Simultaneous derivation of intensities and weighting functions in a general pseudo-spherical discrete ordinate radiative transfer treatment, *J. Quant. Spectrosc. Radiat. Transfer*, **75**, 129-175, 2002.

Spurr, R., LIDORT V2PLUS: a comprehensive radiative transfer package for nadir viewing spectrometers, remote Sensing of clouds and atmosphere, Proceedings SPIE conference 5235, Barcelona, Spain, September 2003.

Spurr, R., D. Loyola, W. Thomas, W. Balzer, E. Mikusch, T. Ruppert, M. van Roozendael, J.-C. Lambert and T.V. Soebijanta, GOME Level 1-to-2 Data Processor Version 3.0: A Major Upgrade of the GOME/ERS-2 Total Ozone Retrieval Algorithm, *Applied Optics* (submitted), 2004.

Spurr, R. J. D., Discrete Ordinate Theory in a Stratified Medium with First Order Rotational Raman Scattering; a General Quasi-Analytic Solution, paper in preparation, 2004.

Thomas, G., and K. Stamnes, Radiative Transfer in the Atmosphere and Ocean, 1st ed., Cambridge University Press, 1999.

Tuinder, O. N. E., R. de Winter-Sorkina, and P. J. H. Builtjes, Retrieval methods of effective cloud cover for the GOME instrument: an intercomparison, *Atmos. Chem. Phys*., **4**, 255-273, 2004.

Van Geffen, J. H. G. M., and R. F. van Oss, Wavelength calibration of spectra measured by GOME using a high-resolution reference spectrum, *Applied Optics*, **42**, 2739-2753, 2003.

Van Oss, R. F, R. H. M. Voors, and R. J. D. Spurr, Ozone Profile Algorithm, OMI Algorithm Theoretical Basis Document, Volume II, OMI Ozone products (P. K. Bhartia ed.), ATBD-OMI-02, Version 1.0, September 2001.

Van Roozendael, M., V. Soebijanta, C. Fayt, and J.-C. Lambert, Investigation of DOAS Issues Affecting the Accuracy of the GDP Version 3.0 Total Ozone Product, in ERS-2 GOME GDP 3.0 Implementation and Delta Validation, Ed. J.-C. Lambert, ERSE-DTEX-EOAD-TN-02-0006, ESA/ESRIN, Frascati, Italy, Chap.6, pp.97-129, 2002.

Vountas, M., V. V. Rozanov, and J. P. Burrows, Ring effect : Impact of rotational Raman scattering on radiative transfer in earth's atmosphere, *J. Quant. Spectrosc. Rad. Transfer*, **60**, 943-961, 1998.

Wellemeyer, C. G., S. L. Taylor, C. J. Seftor, R. D. McPeters, and P. K. Barthia, A correction for total ozone mapping spectrometer profile shape errors at high latitude, *J. Geophys. Res.,***102**, 9029-9038, 1997.

Wenig, M., S. Kuehl, S. Beirle, E. J. Bucsela, B. Jaehne, U. Platt, J. Gleason, and T. Wagner, Retrieval and analysis of stratospheric NO_2 from the Global Ozone Monitoring Experiment, *J. Geophys. Res.*, **109**, D04315, doi:10.1029/2003JD003652, 2004.